Master's Thesis

Designing a new battery system using NaCl aqueous solution as cathode

Sangmin Park

Department of Energy Engineering

(Battery Science and Technology)

Graduate School of UNIST

2016

Designing a new battery system using NaCl aqueous solution as cathode

Sangmin Park

Department of Energy Engineering
(Battery Science and Technology)

Graduate School of UNIST

Designing a new battery system using NaCl aqueous solution as cathode

A thesis/dissertation
submitted to the Graduate School of UNIST
in partial fulfillment of the
requirements for the degree of
Master of Science

Sangmin Park

1. 13. 2016

Approved by

Advisor
Youngsik Kim

Designing a new battery system using NaCl aqueous solution as cathode

Sangmin Park

This certifies that the thesis/dissertation of Sangmin Park is approved.

1. 13. 2016

signature

Advisor: Youngsik Kim

signature

Nam-Soon Choi

signature

Seok Ju Kang

Contents

Abstract

The importance of Electrical Energy Storage (EES) for integration with renewable sources has increased gradually in accordance with rising environmental concerns and energy demands. Although research and development in EES technologies has been progressing, some challenges, such as improved performances, cost, location, etc., still remain before they can be successful. The cost-competition is expected to significantly affect the broad market penetration of EES.

The eco-friendly seawater battery, employing seawater to a cathode material, is cost-effective, thus addressing the cost issue. As a seawater cathode provides Na ions of the energy source continuously and finally, a seawater battery can have high energy density despite having low salt (NaCl) concentration (~0.46 M). That is to say, it should be located near the ocean. In addition, renewable sources, possibly integrated with the seawater battery, are limited owing to the locational constraint.

Herein, a rechargeable saltwater battery is proposed for the first time, which utilizes NaCl aqueous solution as an active material while it has typically served as electrolyte to conduct ions, in batteries or electrolysis. Using cheap and safe saltwater as catholyte allows the battery to be located anywhere, and also offers a significant reduction in production costs which is one of the requisitions for large-scale EES systems. In addition, changing salt levels in water enables the control of the working potential of the cell and energy density (up to 423 Wh/kg at 6 M NaCl). This ultimately provides the flexibilities of the saltwater battery for different applications.

The cell design and components (e.g. change of material components) significantly affected its electrochemical performances. Thus, this research also focused on designing the new cell and the key components (a solid electrolyte and a carbon-based cathode electrode) to test saltwater cathode. The electrochemical mechanism and performances were therefore investigated. In addition, some catalysts were applied to improve cell performances. Lastly, a cost analysis of a saltwater battery was examined, by comparing it to other batteries, to demonstrate its feasibility as a next-generation EES technology.

List of figures

Figure 38. XRD patterns of the pristine NASICON and after 50 cycles. Although the peak intensities changed slightly, no noticeable peak shift was observed between the two spectra, revealing the stability of NASICON in saltwater during cycling.

Figure 39. SEM images of carbon felt (a) with and without catalysts such as (b) Pt/C and (c) Vulcan.

Figure 40. Electrochemical test to investigating influences of catalysts on electrochemical erformances of saltwater battery. (a) Galvanostatic charge and discharge voltage curve at 0.01 mA/cm^2 for 180 hours (3 cycles) with half-cells of Na|1M saltwater. (b) Power density at different current density from 0.01 to 0.75 mA/cm^2.

Figure 41. Comparison of cost for various battery systems. Energy cost ($/kWh) versus power cost ($/kW) using data from the DOE/EPRI 2013 Electricity Storage Handbook. The cost of saltwater battery (red star) was evaluated using 5 M saltwater as the catholyte.

List of tables

1. Introduction.

1.1. Needs for Electrical Energy Storage (EES) and its technologies.

A large portion of all energy consumption is electrical energy, and electricity demand is increasing constantly (Fig. 1) [1]. Fossil fuels, such as coal or oil, have provided the highest amounts of electrical energy (~40% in 2014) [2]. However, the use of fossil fuels has contributed significantly to global warming by generating greenhouse gases (CO_2, CH_4, N_2O and fluorinated gases) and the international agreements of the United Nations Framework Convention on Climate Change (UNFCCC) to reduce mainly CO_2 gas emissions have been adopted by many countries. Accordingly, a big investment in low-carbon technologies at the national level is expected.

These environmental concerns, as well as growing energy demands, is likely to boost interest in producing electricity from renewable sources [3,4]. Indeed, experts estimate that, by 2030, worldwide electricity power generation from renewable energy sources will increase by around three times 2011 levels, as shown in Fig. 2 (ref. 5). Renewable sources, such as solar and wind, however, are variable; and renewable power generation, dependent on their sources, provide only intermittent electrical energy. Fig. 3 shows solar generated electricity during the daytime, but much less electrical energy is generated on cloudy days [5]. Furthermore, power generation by renewable sources are often localized. To address the intermittence of renewable energy, electrical energy storage (EES) will be required [5,6,7].

For the successful commercialization of EES, the cost and performance of EES technologies must be competitive with conventional technologies (e.g. the gas combustion turbine). The performance required of EES is different in applications, as shown in Fig. 4 (ref. 5). For example, to manage energy, by such methods as peak shaving or load shifting, bulk energy up to MWh is required with discharge durations of few hours at a specified power [7,8]. In contrast, a long cycle life is important rather than long-time storage in case of regulating frequency and a quick response is required for ESS integrated into renewable power. Cost is a crucial factor in broad market penetration. This is generally expressed in capital costs, such as unit cost of energy and unit cost of power. In addition, safety and low-maintenance are required for EES to be used as utility assets.

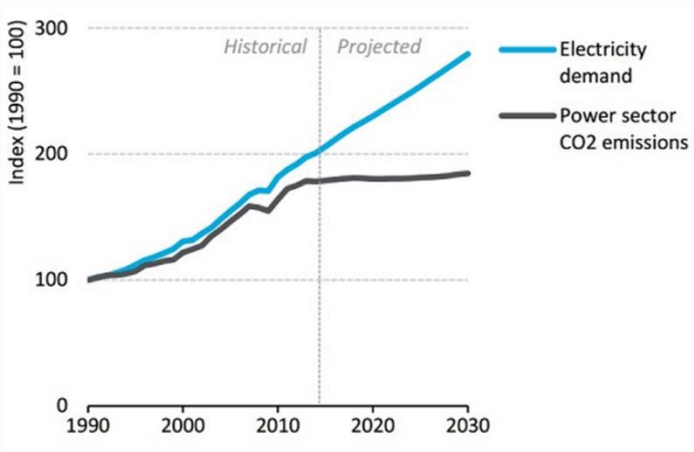

Figure 1. World electricity demand and total CO_2 emissions since 1990.

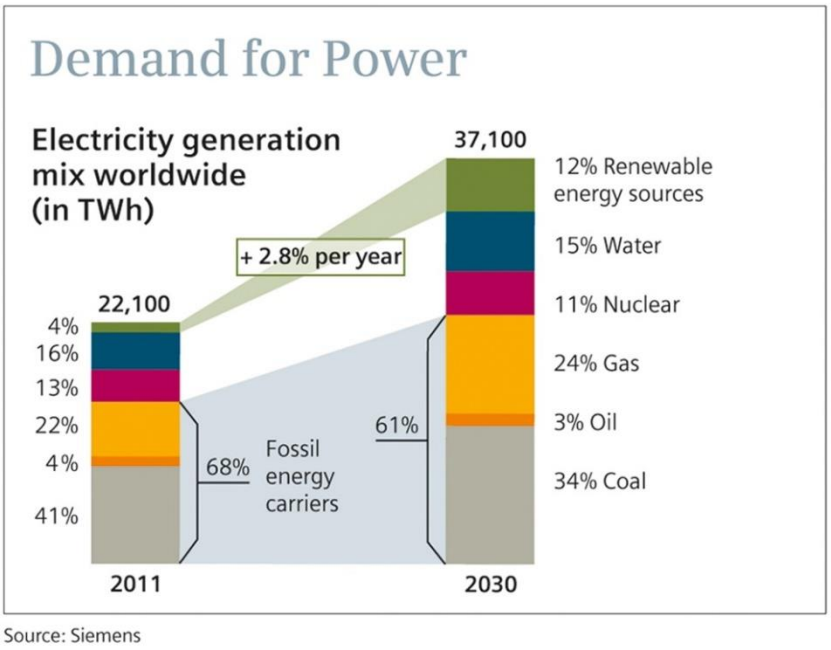

Figure 2. Global electricity generation in 2011 and prediction of that in 2030.

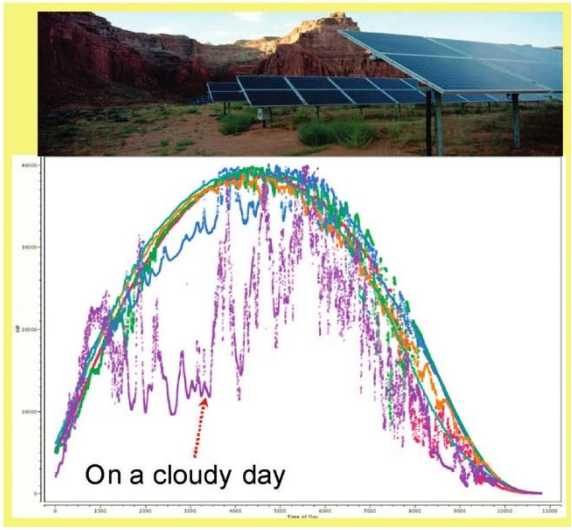

Figure 3. Solar energy profiles for 6 days in Spain. Energy harvesting relied on renewable sources and the renewable power generation provided intermittently electricity.

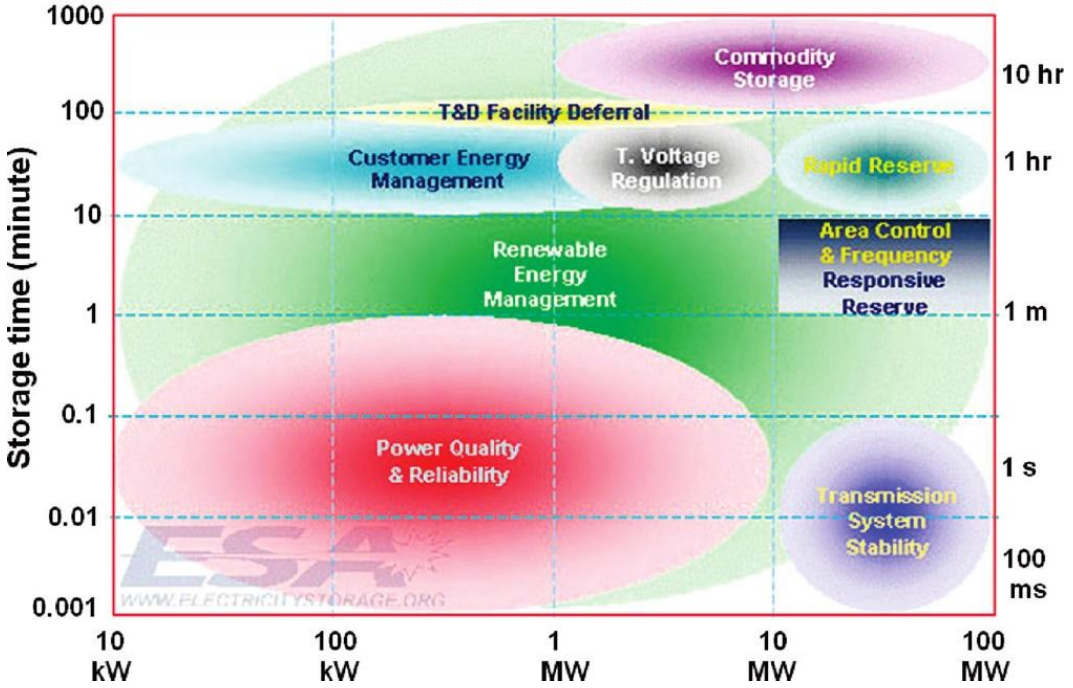

Figure 6. Power and discharge time for various applications.

1.2. Battery Energy Storage systems (BESS).

There are several types of Electrical Energy Storage (EES) technology and those are categorized by how the electricity is stored (Fig. 5) [5,9]. The first group stores electrical energy directly with the use of, for example, capacitors, which have high efficiency and discharge for short time. Another group stores electrical energy by converting it to other forms, such as kinetic, potential or chemical energy. Above all, Pumped Hydro Storage (PHS) technology has been operated worldwide because of its low cost and large capacity. However, the installed site of PHS is restricted and the construction takes long periods; of up to 8 years [5,8]. The reaction time, furthermore, requires up to 10 minutes and in this respect, PHS plants are not suitable for the integration of various renewable energy sources.

Battery Energy Storage Systems (BESS), or batteries, store electrical energy, which is converted from chemical energy, and vice versa (Fig. 6) [10]. Growing attention has been given to these technologies, because of their good lifespan, high energy efficiency, low pollutants and flexible energy and power densities. For example, the desired power densities (current density × voltage) can be obtained by staking electrochemical cells in series and in parallel. In addition, EES are somewhat smaller than other storage systems (i.e. CAES, PHS) so that it is suitable for renewable power plants [5]. Thus, many types of batteries have been researched and developed over the last century. Some of them are available for commercialization and some are in the early stage of research. This part, therefore, addresses further details of representative EES technologies.

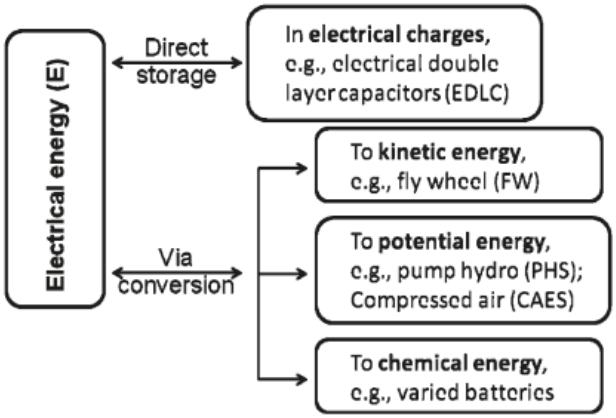

Figure 5. Categorization of electrical energy storage (EES) technologies with respect to form of stored energy.

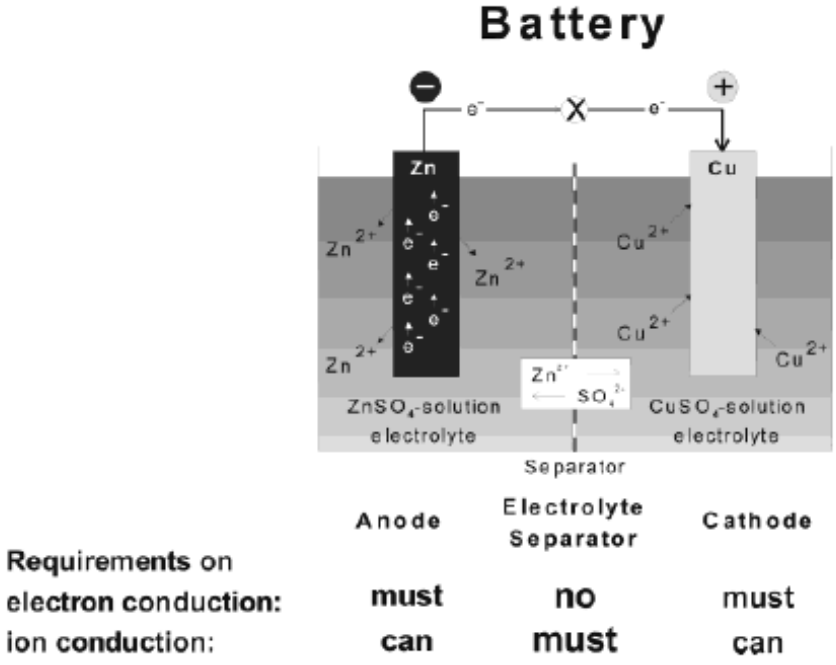

Figure 6. Schematic diagram of a representative battery (such as voltaic cell, Daniel cell or galvanic cell) under discharge process.

1.2.1. Available BESS technologies.

The most promising batteries in terms of commercial availability are Lithium-ion batteries (LIB), Sodium-sulfur (NaS) batteries and redox-flow batteries (RFB) (Fig. 7) [6]. Their pros and cons are quite distinct in accordance with each design and working mechanism, and thus followings focus on that.

As shown in Fig. 7a, LIB consists of cathode (i.e. lithiated metal oxide), electrolyte (of organic solution dissolved Li salt) and anode (i.e. Li intercalated material such as graphite). When it is charged, Li ions transfer from cathode material to anode material via the electrolyte. And the reverse process occurs on discharge. The huge success of LIB in the portable device market has been achieved due to good electrochemical performance, such as high voltage with low redox potential ($E°(Li^+/Li)$= -3.04 V *vs*. SHE) and high energy density (250-300 Wh/kg) and long service lifetimes (2-10 years). Such good battery performance and steadily increasing demand may induce a strain on Li-production capability and increase its market price in the long term, which in turn limits its application in large-scale storage systems [6,11]. The price rise in Li sources has been expected as demand for of lithium in portable electronic devices and as a possible power source for electric vehicles (EV) will increase (Fig. 8) [12].

In contrast, Na is abundant. Na is not only low cost, but also retains suitable potential ($E°(Na^+/Na)$= -2.71 V *vs*. SHE) so that it is appropriate to be used in stationary energy storage systems (Table 1) [13]. In fact, an NaS battery, used to molten salt (NaCl) as anode material, has been commercialized by NGK since 2003 (ref. 14). Fig. 7b shows the NaS cell, of which cathode and anode are separated by a solid electrolyte of beta-alumina, resulting in a high operation temperature requirement (270-350 ℃). On discharge, Na is oxidized to Na^+ ions at the beta-alumina interface. Ions then transfer through the solid electrolyte to cathode and react with S, which is reduced, and forms Na_2S_5. The charge process occurs in reverse. This battery takes advantage of the high capacity and low cost of cathode (S) and anode (Na) materials. On the other hand, the selection of cell components is limited due to its high temperature operation. Corrosion problems can also occur as sulfur and polysulfide are extremely corrosive [5,15]. As a result, the cost of the cell increases and it is difficult to ensure stability of cell. Accordingly, considerable efforts have made for researchers to develop operation at room temperature [15,16,17,18,19].

A typical RFB, composed of two electrolyte reservoirs (which contain catholyte and anolyte) and an ion-selective separator, is illustrated in Fig. 7c. Among them, the most advanced RFB is the all-vanadium redox-flow battery (VRB). When the electrolytes are pumped from reservoirs and flow through electrodes, the electrical energy is converted from chemical energy on the electrodes (discharge process) or vice versa (charge process). That is, the electrode reaction is very simple due to flowing

electrolyte [20,21]. In addition, active species concentration and reservoir size determines its energy density, and the power density relies on the reaction rate of cathode and anode electrodes [22]. Despite these great advantages, low cost is still required as well as cell performance such as capital cost, life-cycle cost and reliability [5,6].

A few challenges to commercial success remain, although these technologies, including others, have reached commercial or demonstration level. The cost has to be reduced to penetrate the market, and the electrochemical performances have to be achieved [5,6].

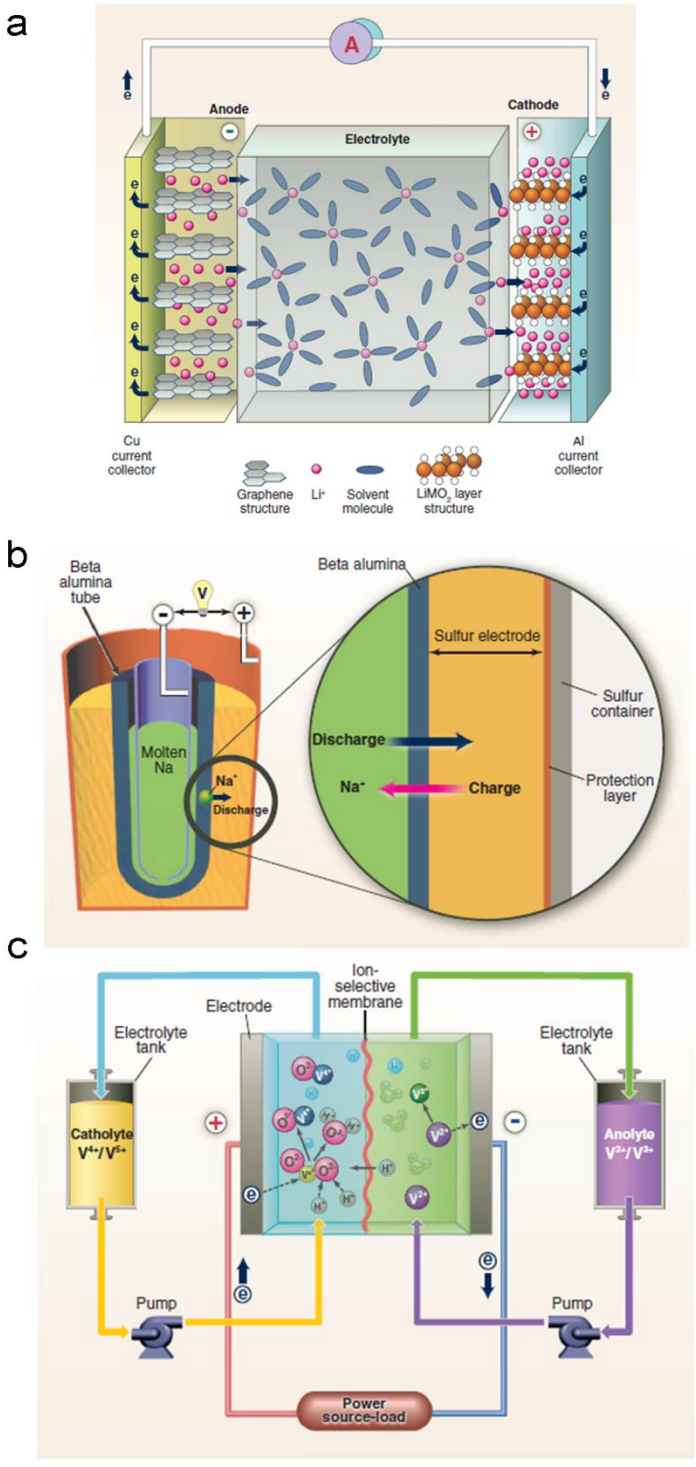

Figure 7. Schematic of available BESS technologies. (a) Lithium-Ion battery (LIB) (b) Sodium-Sulfur (NaS) battery (c) All Vanadium Redox Flow battery (RFB).

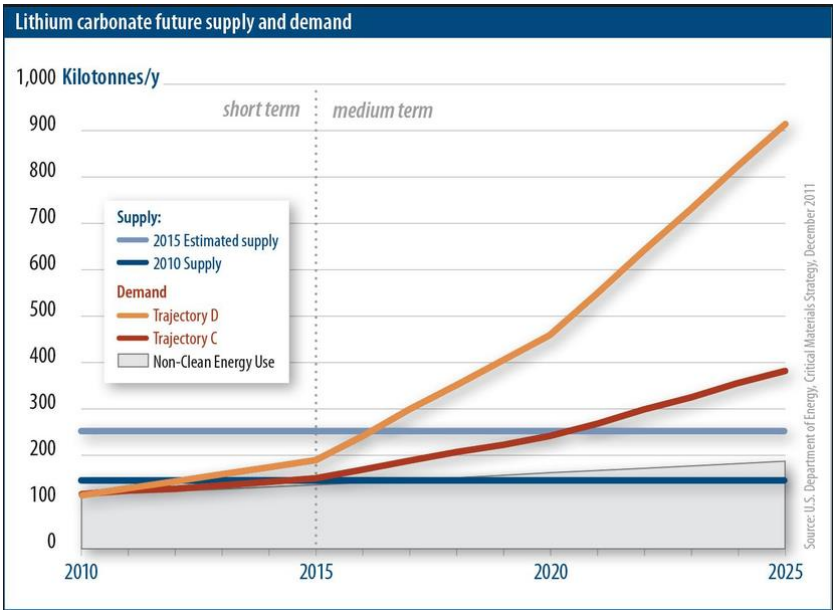

Figure 8. Projected supply and demand for Li_2CO_3 of lithium source.

	Na	Li
Cation radius	97 pm	68 pm
Atomic weight	23 g mol^{-1}	6.9 g mol^{-1}
E_o *vs.* SHE	−2.7 V	−3.04 V
A–O coordination	Octahedral or prismatic	Octahedral or tetrahedral
Melting point	97.7 °C	180.5 °C
Abundance	23.6 × 10^3 mg kg^{-1}	20 mg kg^{-1}
Distribution	Everywhere	70% in South America
Price, carbonates	~2 RMB per kg	~40 RMB per kg

Table 1. Comparison of properties between Na and Li.

1.2.2. Emerging BEES technologies.

Present batteries are insufficient to meet the ESS requirements such as cost (energy and power cost) and performances including energy density, capacity, reliability, durability and safety so that next-generation batteries are going on research [6]. In particular, Li-air batteries, based on electrochemical reaction of Li-O_2, have received attention owing to their high energy density as that of gasoline (1700 Wh/kg) [23,24,25]. The high energy density is attributed that the anode (Li metal) occupies most of each cell volume. There are non-aqueous and aqueous systems in Li-air batteries. Among them, non-aqueous system has been mostly investigated since first reported [26]. However, the non-aqueous system shows high polarization due to side reactions between Li and CO_2 or non-soluble discharge product on air electrode surface and then loss of energy density as shown in Fig. 9 (refs. 24,25,27,28). Moreover, non-aqueous liquid electrolyte can be decomposed during charge and discharge, resulting in thermal runaway [29].

In this respect, aqueous systems have been considered as promising energy storage device despite lower energy density than that of non-aqueous one [24,30,31]. The energy density of aqueous Li-air cell is determined by solubility of LiOH in aqueous electrolyte, which is discharge product in accordance with Li (s) + (1/4)O_2 (g) + (1/2)H_2O (l) → LiOH (aq). And it is inevitable to use protection layer (i.e. LTAP) to separate Li metal of anode and aqueous electrolyte and prevent vigorous reaction of them [30,32]. However, as mentioned above, raw material cost of Li would lead to difficulty to its large-scale commercialization.

As a candidate to replace Li-based devices, Na-based batteries have gained much interest, not only because of natural abundance and low cost of Na, but also the suitable electrochemical potential (E° = -2.71 V *vs.* standard hydrogen electrode, SHE) [15,33]. Especially, aqueous NABs have been considered to possess good reversibility, owing to soluble discharge products (NaOH, table 2) [34,35,36,37] in contrast to aprotic NABs whose discharge products are insoluble Na_2O_2 and/or NaO_2 (Fig. 10) [38]. Nevertheless, poor reversibility on Na metal anode during cycling (repeated plating and stripping) would impede further enhancement of the NABs and cause safety issues, due to high reactivity with the electrolyte and resultant dendritic growth [39,40,41].

Although the next-generation batteries are impressive, these electrochemical performances are insufficient for satisfying the market. Therefore, further research on the specific design of the cell and its components and detailed reaction mechanism must be required.

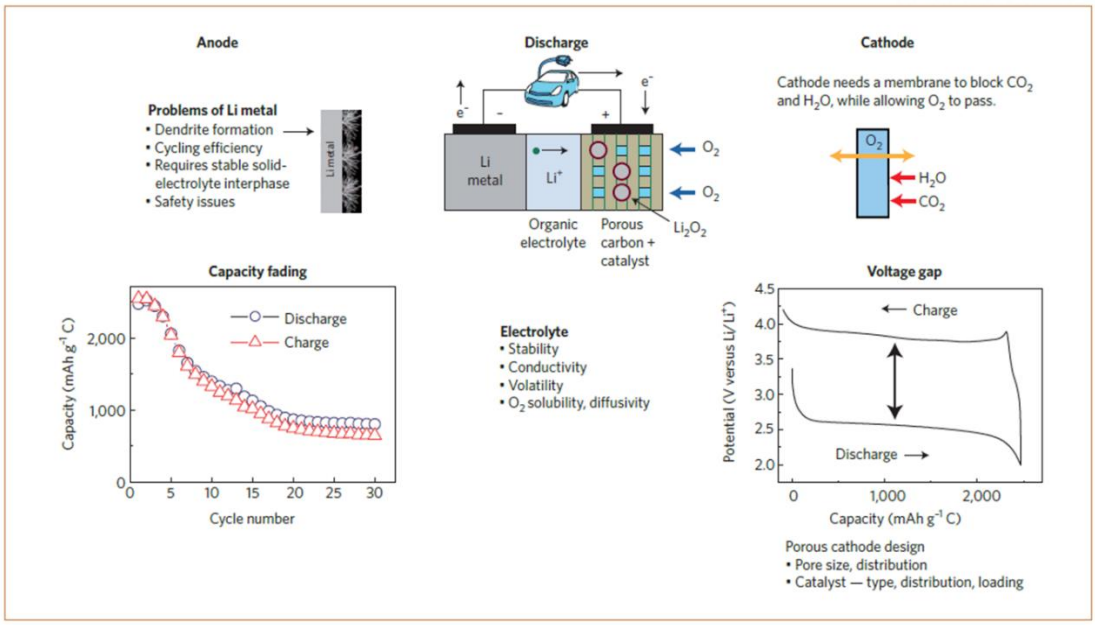

Figure 9. Challenges in the non-aqueous Li-O_2 battery. Graphs for capacity fading and the voltage gap came from the results, tested with Li|1 M $LiPF_6$ in propylene carbonate|MnO_2 nanowires (as a positive electrode).

Battery	Reaction	E_0 (V)	Theoretical energy density ($Wh \cdot kg^{-1}$)		
			Li, Na + $\frac{1}{2}H_2O$	+ $\frac{1}{4}O_2$	+water solvent[a]
Li-air	$Li(s) + \frac{1}{2}H_2O(l) + \frac{1}{4}O_2(g) \rightarrow LiOH(aq)$	3.45	5,800	3,860	440
Na-air	$Na(s) + \frac{1}{2}H_2O(l) + \frac{1}{4}O_2(g) \rightarrow NaOH(aq)$	3.11	2,600	2,090	1,090

[a]Based on solubility at 20°C.

Table 2. Comparisons of Li-air and Na-air batteries for standard cell potentials and theoretical energy densities [34].

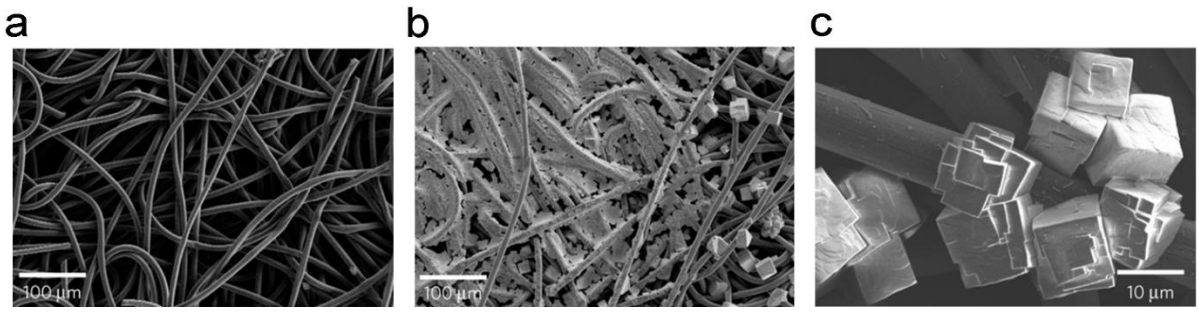

Figure 10. SEM images of cathode electrodes in Na-O_2 cell. (a) Pristine cathode electrode. (b) Oxygen/gas diffusion layer after discharge to 2 mAh at 0.8 mA/cm^2. (c) Discharge products on the carbon fibers at higher magnification.

1.3. A Seawater Battery.

Although the requirement for energy storage from renewable energy has been increasing, the EES technologies, considered as potential candidates, have challenges in penetrating the broad market [5]. Perhaps the most significant issue is the cost of those devices; and so it must be reduced. In this regard, the seawater battery, proposed by our research group [42,43,44], can fulfill the market expectations. The novel rechargeable battery utilizes seawater as a cathode material, or more precisely, a sodium source.

The cathode contains Na ions as shown in Fig. 11a and thus, the seawater battery could work with metal-free anode material such as hard carbon and Na insertion materials. Seawater is abundant and very eco-friendly, so it has price competiveness as a potential stationary energy storage system. The design of the seawater cell and its electrochemical mechanism are shown in Fig. 11b, c. The catholyte of seawater can provide sodium ions, like cathode material in a sodium ion battery, and is separated from an anode compartment by a NASICON ($Na_3Zr_2Si_2PO_{12}$), which has the highly ionic conductivity of ~10 mS/cm. The electrochemical reactions are shown as follows [42]. :

Charge : $NaCl\,(aq) \rightarrow Na^+\,(aq) + 2Cl_2\,(g) + 4e^-$ $E^o = 4.07$ V

Discharge : $4Na^+\,(aq) + 2H_2O\,(l) + O_2\,(g) + 4e^- \rightarrow 4NaOH\,(aq)$ $E^o = 3.11$ V

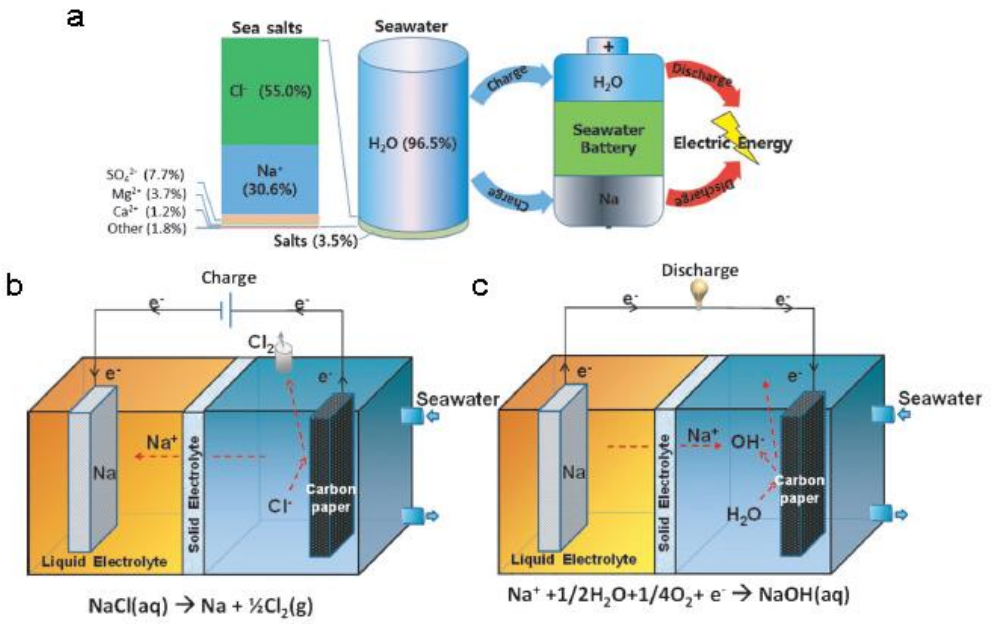

Figure 11. (a) Composition of seawater containing ~0.46 M of NaCl. Schematic diagram of a seawater battery on (b) charge process (chlorine evolution reaction) and (c) discharge (oxygen reduction reaction).

During charging of the seawater battery, the Na^+ ions migrate from cathode to anode through NASICON as the chlorine gas is evolved. The oxygen evolution reaction (OER, E^o =3.94 V) is thermodynamically more favorable than the chlorine evolution reaction (CER, E^o =4.07 V) but the OER is generally known as showing high overpotential [45,46]. Thus, the charge voltage as shown in Fig.12a is practically involved in CER, compared to OER. The CER during the charging process was identified by investigating reduced chlorine and sodium ions, in sea water, as a function of charging time (Fig. 12b, c).

On discharge, the oxygen reduction reaction is observed as above equation. The dissolved oxygen and water is reduced and the Na^+ ions accordingly transfer from anode to cathode. Although the water molecules can be reduced without oxygen, the measured discharge voltage was higher than in that of the water reduction (E^o =1.88 V) which is probably attributable to the participation of oxygen. A result of discharging the cell with bubbling Ar/H_2 gas, which made the oxygen-free environment, showed that the discharge voltage was actually similar to 1.88 V (ref. 42).

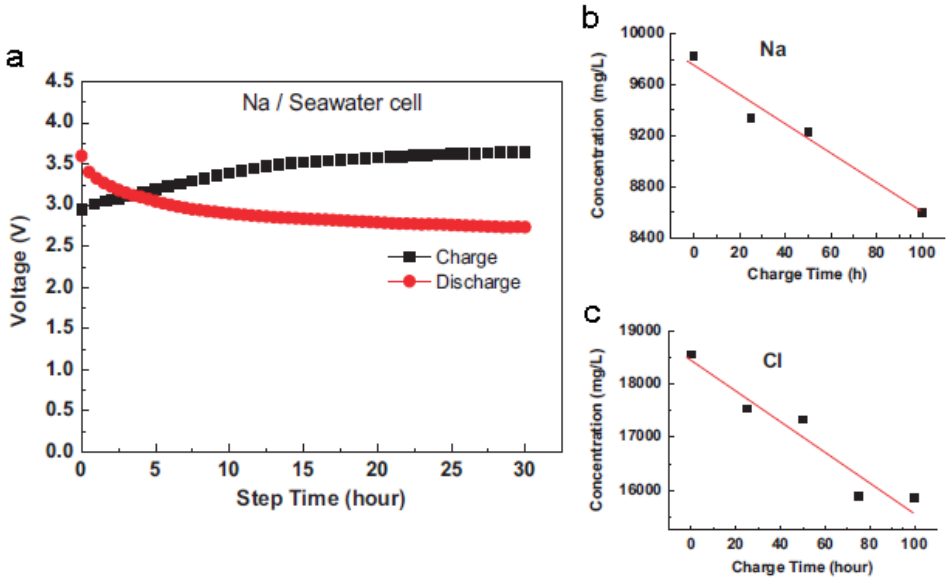

Figure 12. (a) Charge and discharge voltage profile of a seawater cell constructed with a Na|seawater cell at the current rate of 0.01mA/cm^2. Remaining (b) Na^+ and (c) Cl^- ions in seawater as a function of charging time [43].

The rechargeable seawater battery can use anode materials as a negative electrode like sodium ion batteries (NIB) [43]. There were reported to this day that hard carbon and Sn-C electrodes were employed since hard carbon can reversibly store Na ions at low voltages (under ~1.0V) [47,48] and Sn-based materials provide high capacity [49,50]. Fig. 13 shows the electrochemical performances of rechargeable seawater cells with those anode electrodes [44]. Both of them indicated irreversible capacity at early cycles. This was attributed to form a solid-electrolyte interface (SEI) layer on the surface of those electrodes. After that, they showed stable cycle performances of their discharge capacities up to 30 cycles. The Sn-C electrode, especially, retained two times higher the reversible capacity of hard carbon. As a result, it is demonstrated that seawater can play a successful role as an open-cathode by providing infinite Na-ions.

As mentioned in the previous part, electrochemical energy storage devices (EES or batteries) have received growing interest, as the energy and power densities is suitable for use by renewable energy sources and they are not limited to certain locations. The use of seawater, however, presents the disadvantage of geographical limitation. , which has to be located near ocean. Thus, it restricts to apply it to energy production with various renewable sources. Furthermore, the seawater cell has low energy density according to Na ions (~0.46 M) dissolved in seawater [51].

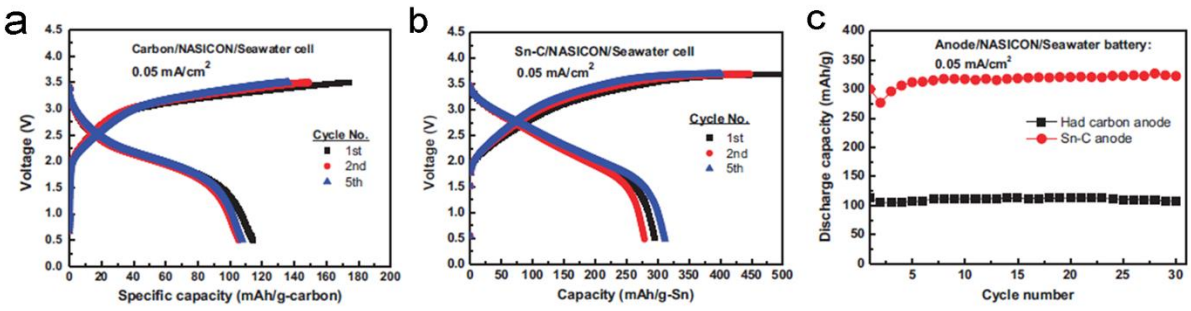

Figure 13. Charge and discharge voltage profiles of rechargeable seawater cells composed of (a) hard carbon|seawater (b) Sn-C|seawater at the current rate of 0.05 mA/cm^2. (c) Cycle performances of the cells.

1.4. Purpose of my research work.

The main challenge for broad market shares of ESS products is high cost as to meet the commercial requirements through recent developments of the various technologies. An eco-friendly seawater battery, employing seawater as an energy source, is proposed as a new approach to address the issue. Na-ions of an energy source are obtained consistently from seawater and the battery can provide lots of Na-ions with low cost. However, using seawater limits installation-sites to nearby the ocean. Alternatively, the energy density is reduced, owing to low sodium concentration (~0.46 M) [51], when the battery is located far from the ocean and the seawater is transported. It is, therefore, difficult to applied the seawater battery to various types of renewable power plant.

In this study, NaCl dissolved in aqueous solution or, in other words, saltwater, was used as cathode material. Saltwater batteries can be found easily, but most of these only utilized saltwater as electrolyte, which is ion-conductive material [52,53,54]. However, a rechargeable saltwater battery, proposed here, employs saltwater to ultimately provide Na sources as much as dissolving NaCl in water (up to 6 M). Various concentrated saltwater enables adjusting energy density (up to 423 Wh/kg per a cell) according to applications. There are also some advantages of no-limited locations and cost satisfaction as EES.

To investigate the potential of a saltwater battery as a next electrical energy storage technology, this research focused on three objectives as below:

Firstly, to design a novel cell to store electrical energy by using saltwater. In particular, solid electrolyte and positive current collector as key components will be further investigated in respect to their role, requirements and influence on the cell performance.

Second, the cell operation mechanism and electrochemical performances for a rechargeable saltwater battery will be studied with Electrochemical and other characterizations.

Third, cost analysis will be conducted to examine prices-competitiveness of a saltwater battery. And it will refer to material costs for the battery and DOE/EPRI 2013 Electricity Storage hand book [7].

2. Experimental Methods

2.1. Synthesis and preparation of ceramic electrolytes.

A sodium conductive solid electrolyte with $Na_3Zr_2Si_2PO_{12}$ known as a Hong-type NASICON was synthesized with a solid state reaction [55]. The starting materials of $Na_3PO_4{\cdot}12H_2O$ (Daejung, 99 %), SiO_2 (Daejung, 99 %) and ZrO_2 (Kanto, 99.9 %) were mixed at 300 rpm for 2 hours by ball-mill machine in ethanol and dried at 80 ℃. The mixture was calcined in an Al_2O_3 crucible in air in two steps as follows: The first-calcination was done at 400 ℃ for 5 hours,followed by 1100 ℃ for 12 hours. The first-calcined power was ground before the second calcination. After all calcination steps, the synthesized NASICON was crushed with mortar and milled in a planetary mill with zirconia balls at 250 rpm for 30 min. The dried power was made into disks of about 1.3 mm thickness and 2.1 cm diameter by uniaxial pressing (1 ton). The pellets then underwent cold isotactic pressing (CIP) at 2.5 ton. Dense NASICON pellets ware sintered on Pt sheets at 1280 ℃ for 10 hours under atmosphere.

A Von Alpen-type NASICON of $Na_{3.1}Zr_{1.55}Si_{2.3}P_{0.7}O_{11}$ was prepared by the same process, except as follows. The powder was synthesized with $Na_3PO_4{\cdot}12H_2O$ (Daejung, 99 %), Na_2CO_3 (Wako, 99.5 %), SiO_2 (Daejung, 99 %) and ZrO_2 (Kanto, 99.9 %) and just the first-calcination was processed at 1250 ℃ for 10 hours. The synthesized powder was uni-axially pressed at 1 ton in order to shape pellets, which were sintered on a Pt sheet at 1300 ℃ for 2 hours.

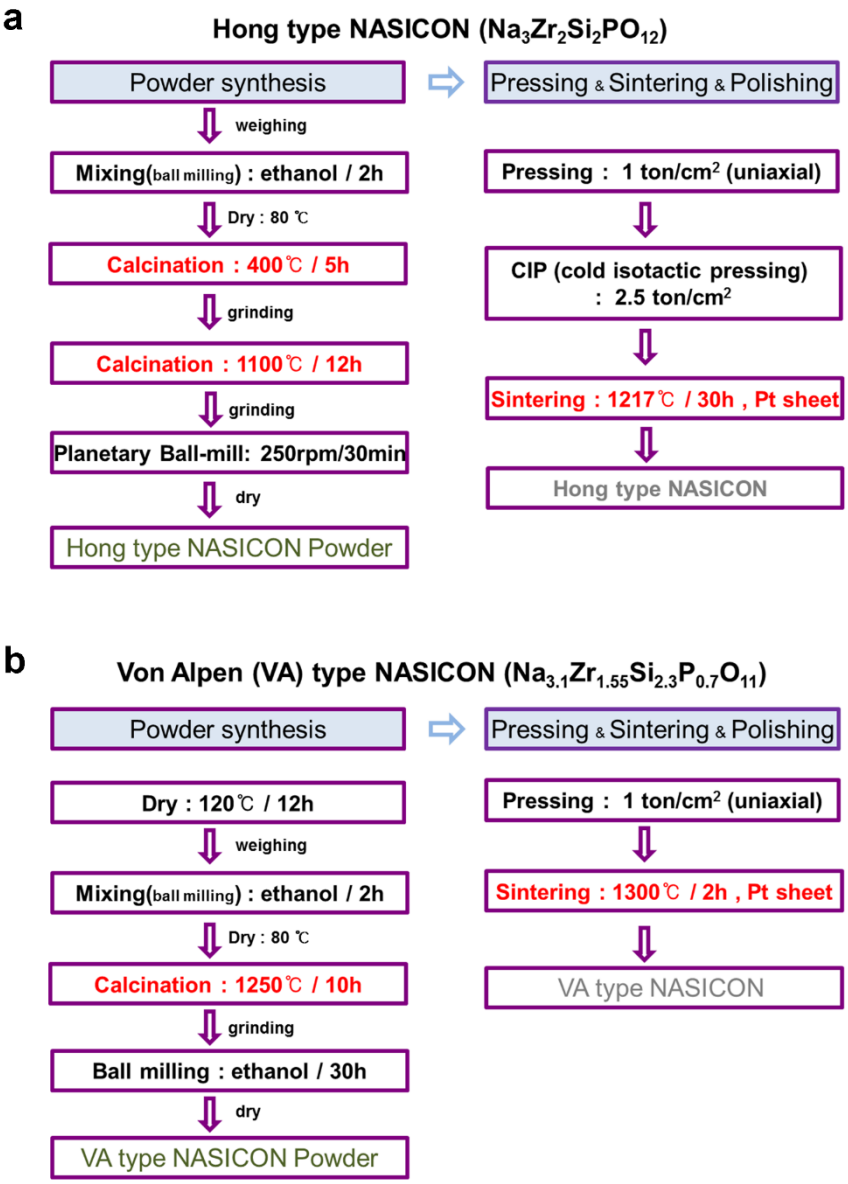

Figure 14. Synthesis and fabrication process of NASICONs.

2.2. Preparation and configuration of rechargeable saltwater battery.

For the catholyte, 60 mL saltwater was prepared by dissolving NaCl (Sigma Aldrich) into deionised water at various concentrations of 0.4–5 M.

For the current collector of the cathode side, a Ti mesh (Wooilmetal Corp.) and carbon electrodes were used. The 4 types of carbon electrodes were hydrophobic carbon paper (JNT Co., Ltd.), neutral hydrophilic carbon paper (Fuel Cell Store), graphene oxide carbon paper and carbon felt (XF30A, Toyobo), which was heat-treated under 500 ^{o}C for 2 hours to change the surface property from hydrophobic to hydrophilic. The graphene oxide carbon paper was made as follows. First, carbon paper (2 cm $\times$ 2 cm, JNT Co., Ltd.) was pre-treated by serum albumin protein (0.5 wt% in D.I water, Sigma Aldrich) to make an amphiphilic surface on carbon paper. Carbon paper was dipped in the protein solution followed by continued stirring for 12 hours and the pre-treated carbon paper was slightly washed by D.I water and dried in a conventional oven at 60 ^{o}C for 2 hours. Graphene oxide (GO) was synthesized by a modified Hummers method [56]. The 0.01 g of the GO sheet was dispersed in the 20 ml of D.I water through the horn sonication to result in 0.5 mg/mL GO solution. And the protein coated carbon paper was dipped in GO solution and also shaken for 18hours to allow the GO sheet to self-assemble on the carbon paper. Finally, the GO self-assembled carbon paper was washed by D.I water and dried in a conventional oven at 60 ^{o}C for 2 hours. A solid electrolyte of NASICON ($Na_3Zr_2Si_2PO_{12}$), ground with emery paper, was consistent with thickness (0.8 mm) and area (~2 cm^2, diameter of 8 mm).

An anode part, where NASICON was sealed in the air, was injected with organic electrolyte of 1 M $NaCF_3SO_3$ (Sigma Aldrich) in tetra ethylene glycol dimethyl ether (TEGDME, Sigma Aldrich) and assembled in the glove box within high impurity Ar gas and water at less than 1 ppm. Na metal, used as one of anode materials, was attached to a Ni mesh (Wooilmetal Corp.) of 9 mm^2 in the glove box. The hard carbon electrode was prepared from a slurry of hard carbon (MeadWestvaco Corporation), carbon black Super-P (TIMCAL), and polyvinylidene fluoride (PVdF, Sigma Aldrich) at the weight ratio of 80:10:10. The slurry was coated on Cu foil (14 μm thick) with a doctor-blade, and dried in a convection oven. Finally, the electrode was roll-pressed and dried in a vacuum oven. The loading level of hard carbon was approximately 2.44 mg/cm^2. The assembled cells which consisted of Ni tap|anode|organic electrolyte|NASICON|saltwater|positive current collector|Ti mesh were immersed in saltwater for electrochemical tests.

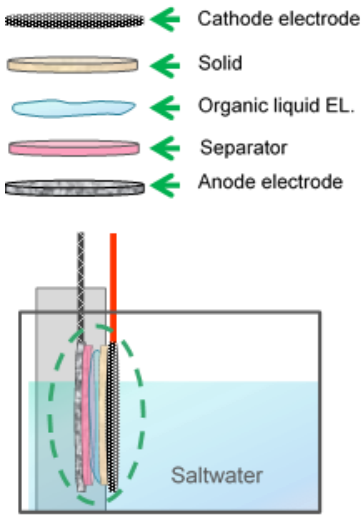

Figure 15. Configuration of pouch cell type saltwater battery.

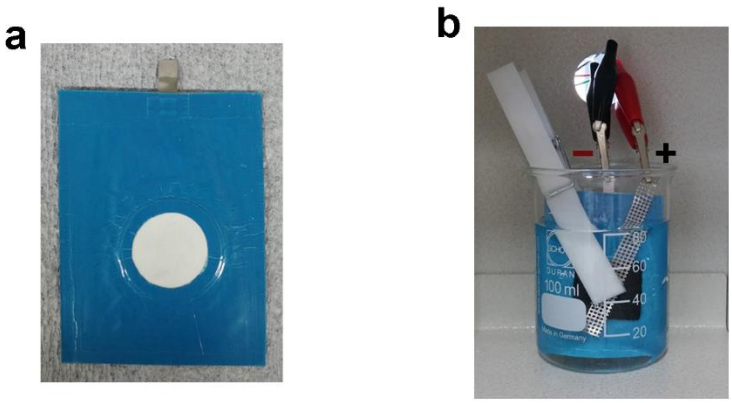

Figure 16. Digital images of saltwater battery. (a) Anode compartment constructed with anode electrode|organic electrolyte|polymer separator|NASICON. (b) Charge and discharge with assembled saltwater battery.

2.3. Preparation catalyst and coating method [37].

There were three different catalysts coated on the carbon felt including Pt/C (Alfa Aesar, 50 wt% Pt) and Vulcan (Fuel Cell Store, XC72R). The prepared catalysts and PVDF binder (Sigma Aldrich) weighed, respectively, at a ratio of 90:10 weight percent. And N-methylpyrrolidone (NMP) was added to the powder and mixed with Thinky Mixer (AR-100, Thinky Co., Ltd.) for 5 minutes to make slurry. Carbon felt (XF30A, Toyobo), heated at 500°C for 2 hours was dipped in the slurry and mixed with the Thinky Mixer for 1min before being dried at 80 °C for 5 hours.

2.4. Electrochemical measurements.

The electrochemical properties of saltwater batteries were measured by a battery cycler (WBCS 3000, Wonatech) at room temperature. A galvanostatic method under 0.025 mA/cm^2 was conducted to confirm characteristics of charge and discharge voltage. Cyclic voltammograms (CV, BioLogic) of different concentrations of saltwater were investigated with three electrode systems and the CV curves were recorded at scan rates of 10 mV/s. In three electrode cell, the carbon felt was used as a working electrode with Ag/AgCl (3 M NaCl) electrode (0.197 V *vs.* standard hydrogen electrode (SHE)) as a reference electrode and Pt-wire as a counter electrode. To confirm characteristics of charge and discharge depending on salt concentration or catalysts, electrochemical tests were performed under changing current densities from 0.01 to 0.5 mA/cm^2. The hard carbon anode was examined at a current rate of 0.025 mA/cm^2 in a voltage window of 0-2 V *vs*. Na^+/Na over 5 cycles. The full-cell saltwater batteries were tested at a current rate of 0.025 mA/cm^2 with a capacity cut-off (300 mAh/$g_{\text{hard carbon}}$) upon charging and a voltage cut-off of 0.5 V upon discharging. The current rate was estimated with the geometrical area of NASICON (2 cm^2). All potentials in this paper were referenced to SHE.

2.5. Characterizations.

pH measurement (Eutechinstruments) and conductivity measurement (Cyberscan con 11, Eutechinstruments) for cycled cathode solution was observed. The Cl^- ion concentration in saltwater was determined by using ion chromatography systems (Dionex ICS 3000). The densities of solid electrolytes were measured with a gas displacement pycnometry system (AccuPyc 1340, Micromeritics Instrument Corp.). XRD patterns of solid electrolytes were obtained from X-ray diffraction (XRD, D/Max, Rigaku apparatus) with a CuKα X-ray source (λ=1.5406 Å)). After Pt coating on the surface of ceramics, Electrochemical Impedance spectroscopy (EIS, Biology) was conducted with a frequency range of 100 mHz-7 MHz and a voltage amplitude of 14.2 mV. X-ray Photoelectron Spectroscopy (XPS, K-alpha, Thermo Fisher), Raman (alpha300R, WITec), contact angle measurement (Phoenix 300,

SEO), and Scanning Electron Microscope (SEM, verios 460, FEI company) analyses were performed to observe surface wettability properties and the morphology of carbon electrodes. Energy-dispersive X-ray Spectroscopy (EDS, Bruker) and XPS were conducted to identify Na ions on the anode side of Na metal extracted saltwater and cycled hard carbon, which is rinsed with organic solvent (TEGDME) to remove elements of electrolyte on the surface. The condition of catalysts coated on the carbon felt was observed with a Scanning Electron Microscope (SEM, verios 460, FEI company).

3. Results and Discussion

3.1. Design and key components of the saltwater battery.

Saltwater batteries store electrical energy based on the electrochemical reactions of an aqueous NaCl solution, which is easily available at low cost. A new energy conversion device was required to use the saltwater cathode, since commercialized coin cells (i.e. coin cell 2032) are not able to convert saltwater to electrical energy. The schematic in Fig. 17 is a cell design for testing a saltwater cathode. The anode and cathode compartments of a cell are separated by a ceramic solid electrolyte. First, the cathode part is composed mainly of saltwater and a current collector, where the saltwater is used as the energy source of Na^+ ions, as well as the catholyte. The positive current collector provides a large surface area (reaction sites), together with good wettability. Next, the anode part consists of Na metal or sodium-insertion materials (e.g. hard carbon) as the negative electrode and 1 M $NaCF_3SO_3$ in tetra ethylene glycol dimethyl ether (TEGDME) as a liquid organic electrolyte. For the solid electrolyte, a Na super ionic conductor, NASICON ceramic, is used to separate the cathode and anode parts and allow only Na^+ ions to be selectively transported between them. Sealing between cathode and anode is especially important for cell design because non-aqueous electrolyte is generally sensitive to humid conditions and causes safety issues due to its high reactivity with air [57,58,59]. Contact between the anode compartment and cathode electrode is also significant for reducing contact resistance. In this part, solid electrolyte and positive electrodes were mainly studied as key components.

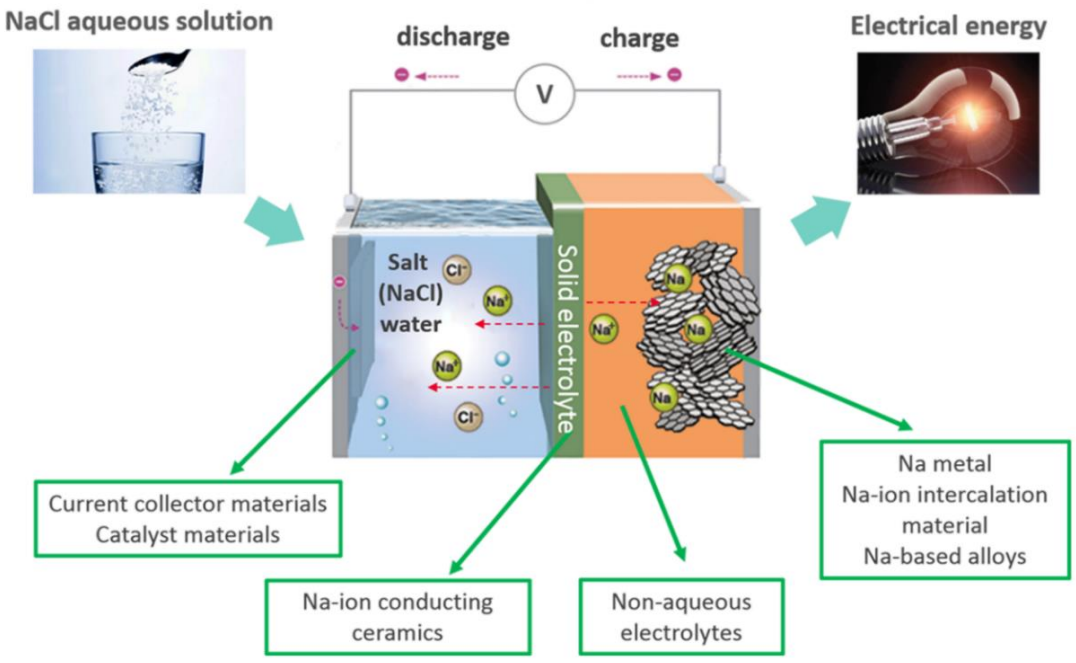

Figure 17. Designed cell structure for using saltwater cathode.

3.1.1. NASICONs as a solid electrolyte.

Solid electrolyte plays a key role in separating the cathode and anode compartments of a saltwater battery. The sodium metal anode can be protected from aqueous cathode. In addition, it offers a wide choice of anode electrodes with suitable organic electrolyte. Solid electrolytes serve as the electrolyte, conducting sodium ions between cathode and anode, and separator, dividing anode from cathode. Therefore, the ceramic separator satisfies suitable water durability as well as high Na-ion conductivity [32,60,61].

Two Na-ion conducting ceramics of Na β″-Al_2O_3 and $Na_3Zr_2Si_2PO_{12}$ (NASICON) were considered as solid electrolytes [62]. Na β″-Al_2O_3 has a two-dimensional structure and exhibits good ion conductivity of ~ 2.0×10^{-3} S/cm at room temperature. NASICON has demonstrated an ionic conductivity up to 2.5×10^{-3} S/cm in a three-dimensional structure [63,64,65]. Although Na β″-Al_2O_3 and NASICON are reported to be moisture-sensitive [66,67,68], NASICON was demonstrated to be stable for 2 months without a big change in its structure and conductivity in a seawater battery. The Na conducting ceramic was considered as a candidate for solid electrolyte.

NASICON is a solid solution of sodium zirposis and it can be divided into two parts: Hong-type and Von Alpen-type, according to its composition [55]. Hong-type NASICON has been known to general composition of NASICON : $Na_{1+x}Zr_2Si_xP_{3-x}O_{12,}$ $0<x<3$, which shows the best Na-ion conductivity at x=2(ref. 69). Earlier studies identified difficulties in preparing pure NASICON without other phases [70], and all the Hong NASICONs consisted of 3 phases including NASICON phase, ZrO_2 phase and glass phase. The appearance of ZrO_2 phase in the structure affects electrical and ceramic properties. For example, ZrO_2 phase increases grain boundary resistance, by impeding transfer of Na ions. These problems led to another formula for the NASICON, called Von Alpen (VA) NASICON [71]. VA NASICON has the general formula, $Na_{1+x}Zr_{2-x/3}Si_xP_{3-x}O_{12-2x/3}$, exhibiting the best conductivity at x~2.2. This composition is deficient in ZrO_2 contents [55] and thus, the NASICON is mostly composed of NASICON and glass (~30 %) phases. But VA NASICON has been reported to be quite unstable in water, resulting from reaction with glass phases and water [68,72,73,74], and the structure and ion-conductivity would be degraded while exposed to water for some time [75].

They were prepared by solid state methods and characterized with SEM, XRD and EIS measurements. The synthesized Hong and Von Alpen (VA) NASICONs did not appreciably differ in the XRD result (Fig. 18). On the contrary, the SEM images of two dense NASICON pellets were a little different, as shown in Fig. 19. Hong NASICON is composed of NASICON phase, ZrO_2 phase and glass phase corresponding to gray grains, white grains and black amorphous phase, respectively [72,76]. The

solid electrolyte had a density of 3.14 g/cm^3 and 96 % of the theoretical density [64]. The microstructure of VA NASICON showed NASICON phase, glass phase and no free ZrO_2 phase. As shown in Fig. 20, the glass phase of the VA materials had a composition with rich Si and low Zr content [55,77]. It has been reported in earlier studies that the Si-rich glass was very unstable. However, there has not been reseach to confirm this [68,72,77].

Fig. 21 shows the Nyquist plot of NASICONs measured by electrochemical impedance spectroscopy at 25 ^oC, which has a semi-circle of bulk resistance and a grain boundary at a high frequency range and inclined a line of interface resistance at a low frequency range [65]. Calculated ionic conductivities of Hong and VA ceramic conductors are similar values of 1.6×10^{-3} and 1.16×10^{-3} S/cm, respectively. Although the conductivities were lower than one of conventional liquid electrolyte, both of them were enough to transfer Na ions fast. In addition, they were non-flammable materials, which were good for safety. Therefore, both conductors are considered to be desirable candidates for solid electrolyte in a saltwater battery.

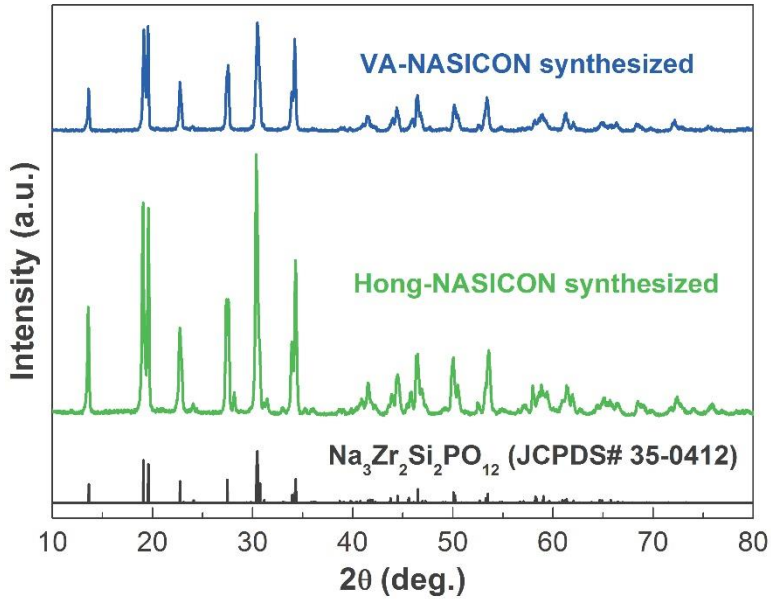

Figure 18. Characterization of NASICONs. XRD patterns of reference (bottom), the synthesized Hong - type (middle) and the synthesized Von Alpen (VA) – type NASICON (bottom) ranging from 10 degree to 80 degree.

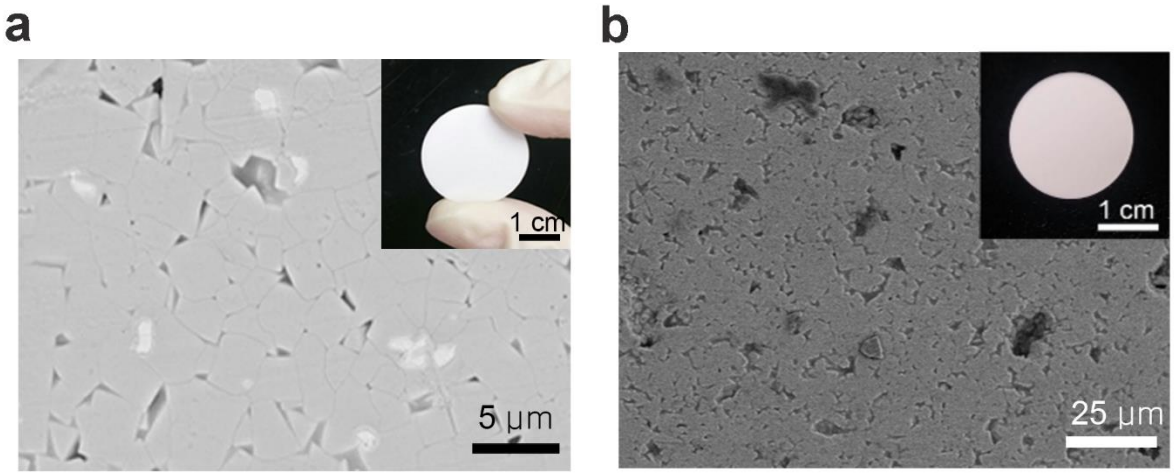

Figure 19. Plan-view SEM-BSE image of (a) Hong-type and (b) Von Alpen-type NASICONs and its digital image (inset).

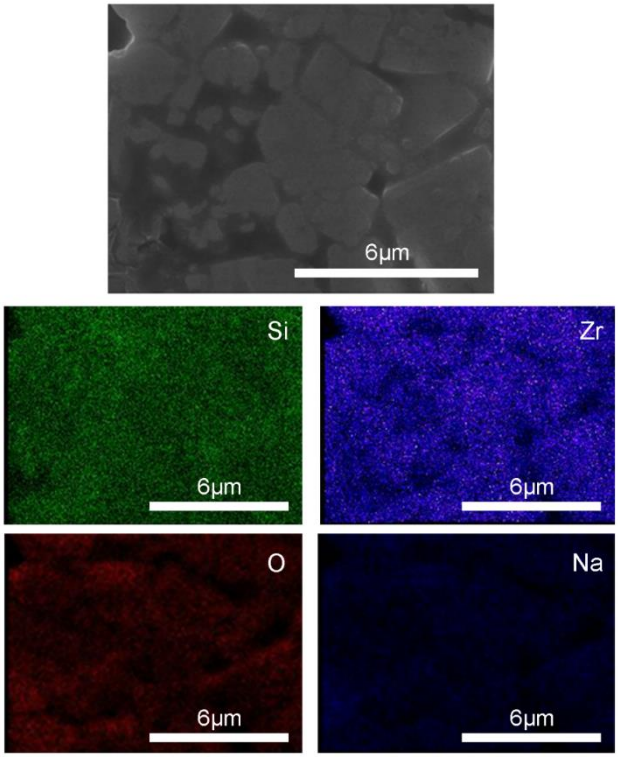

Figure 20. A SEM image of Von-Alpen type NASICON and EDS mapping for elemental composition.

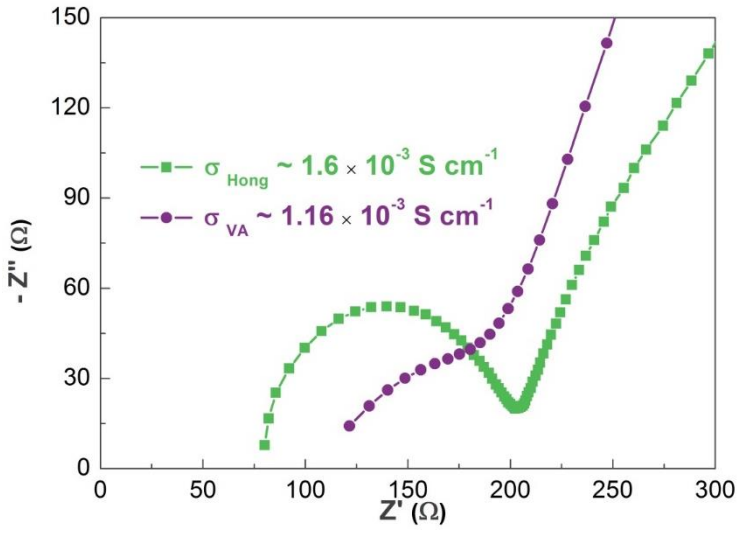

Figure 21. Nyquist plots of the AC-impedance spectrum of NASICONs.

Reacting NASICON with water has been reported elsewhere [68,72,73,75]. When exposed to water, the NASICON was degraded due to ion exchange between Na^+ ions in the structure and hydronium (H_3O^+) ions in the aqueous solution [78]. On the other hand, no one has reported exactly that how long the ceramics can be stable [68,72,77]. To study the chemical stability of the ceramics in water, XRD characterization was utilized after immersion for 60 days in water (Fig. 22). After 60 days, the XRD patterns of Hong NASICON revealed no new peak and no changed structure, as shown in Fig. 21. As a result, the Hong NASICON was anticipated to be stable in aqueous solution for at least 60 days. Unlike Hong NASICON, hydronium NASICON peak was observed in XRD patterns of VA NASICON, which was immersed for 60 days. As mentioned above, formation of hydronium ions in the crystal indicated that the VA NASICON was degraded and the structure could be deteriorated. Although an accurate mechanism for reacting with water has not been reported, it has been suggested in many studies that the reactivity of glass phase with water is a leading cause [72,75,77]. The XRD results show that VA NASICON appears to be much more unstable in aqueous solution than another one agree with earlier studies. Consequently, the Hong NASICON was selected as the solid electrolyte in the saltwater battery.

In order to further study the usage of Hong NASICON as an electrolyte, the impedance spectroscopy was performed after suspension in water (Fig. 23). The bulk resistivity was slightly increased after 60 days immersion, while having similar values for grain-boundary. Accordingly, leaching Na^+ ions from NASICON may have influence on increasing bulk resistivity by reducing charge carriers of Na^+ ions in the crystal. However, it is expected that the Hong NASICON could work successfully in a saltwater battery for at least 60 days, as the calculated ion-conductivity had not dramatically changed from its pristine state for 2 months. The detailed studies on chemical or physical durability of NASICON with water are under way.

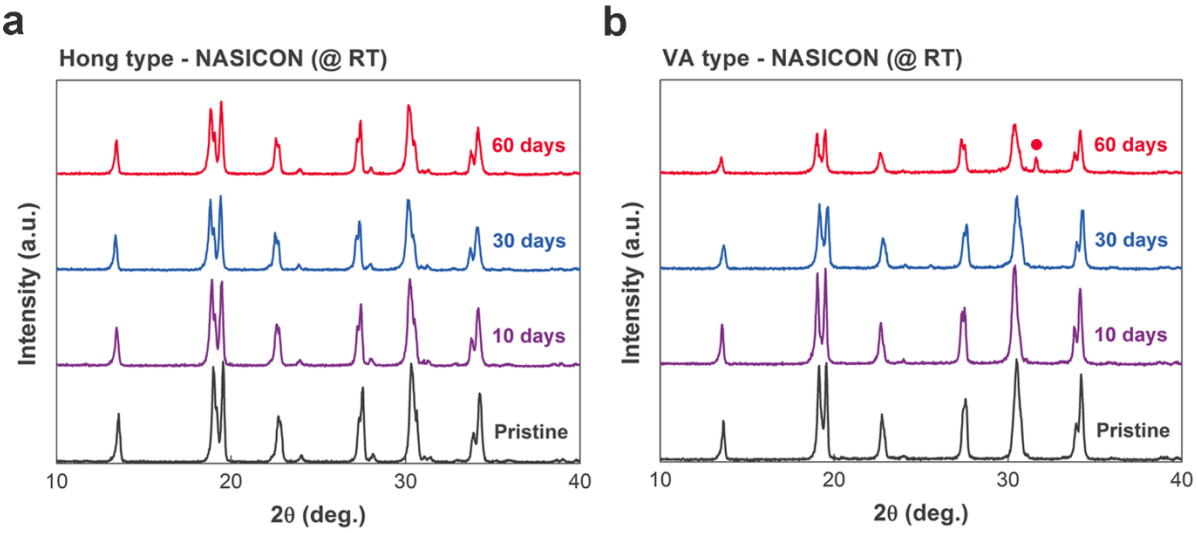

Figure 22. XRD patterns of the (a) Hong-type and (b) Von Alpen-type NASICONs as a function of immersion time in sea water. The red circle indicates a peak of hydronium NASICON [68,78].

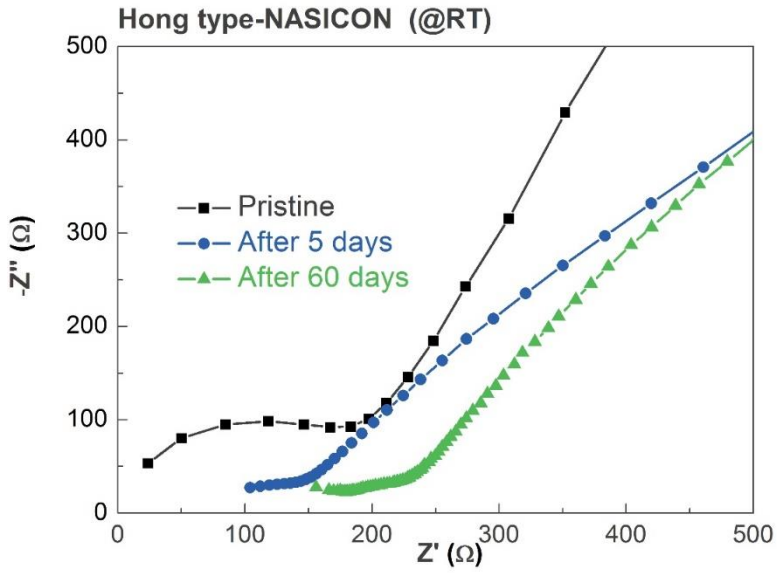

Figure 23. Nyquist plots of the AC-impedance spectrum of the Hong-type NASICON as a function of immersion time in sea water.

3.1.2. Carbon electrodes as a positive electrode.

The cathode side current collector generally serves as an electron pathway. In a saltwater battery, it provides reaction sites for saltwater catholyte. The electrode requires a large surface area, low electronic resistance, suitable porosity and good chemical stability toward electrochemical reactions [79]. The carbon material is also low cost and is a highly suitable electrode for the requirements. It would be generally considered as a current collector in an RFB battery or fuel cell [80,81,82]. Carbon based materials, such as carbon paper or carbon felt was tested as a cathodic electrode in the saltwater battery.

Among the requirements, the wettability property of the electrodes has a great effect on electrochemical performances since the hydrophilic carbon electrode could provide more activation sites and increase electrochemical activity [83]. Second, the contact resistance between a carbon electrode, metal current collector and the anode compartment of the cell must be decreased for stable cell performance [84]. In this part, the behavior according to properties (i.e. hydrophilicity), of carbon electrodes was studied. The carbon paper and carbon felt used as a current collector in the cathode compartment in this study. In the parts of 3.2-3.3 (as a beginning step), carbon paper was utilized and then, carbon felt work with catalysts to improve the cell performances.

Carbon paper (CP) is used as the current collector for saltwater cathode. Commonly, the current collector has to have high surface area and good wettability [79]. However, the carbon paper has designed the diffusion layer of the hydrogen in the fuel cell usually, which has a hydrophobic property [82]. To confirm the difference between neutral hydrophilic and hydrophobic carbon paper, some characterizations were conducted, as shown in Fig. 24. The neutral hydrophilic carbon paper (HCP) was purchased from the Fuel cell store and the hydrophobic paper was obtained from JNTG. Both of them consist of randomly arranged carbon fibers and have a porous structure. There were some particles on the carbon fibers of the hydrophobic carbon paper, while the hydrophilic carbon paper (HCP) was only composed of carbon fibers. The particles were oxidized resin, which was confirmed by a manufacturer. In Fig. 24a and c, the results of XPS and images of the contact angle show that HCP is more wettable than the hydrophobic one. This is because the HCP has a lot of oxygen functional groups on the surface, which contributes to increased wettability of the surface, as shown in the image of contact angle. As mentioned above, the cathode electrode requires good wettability for high electrochemical performance. It is consistent with the galvanostatic discharge curves of saltwater batteries (Na|1 M saltwater), which utilized both types of carbon paper (Fig. 24b). The cell using the HCP shows a stable discharge curve in contrast with another. These results show that the hydrophilic carbon electrode provides numerous reaction sites for catholyte and improves the electrochemical kinetics [80]. As a result, it is obvious that the hydrophilic carbon paper must be selected as a positive current collector.

However, carbon paper is generally used for proton exchange membrane fuel cells (PEMFCs) such that it is difficult to keep on using HCPs continuously.

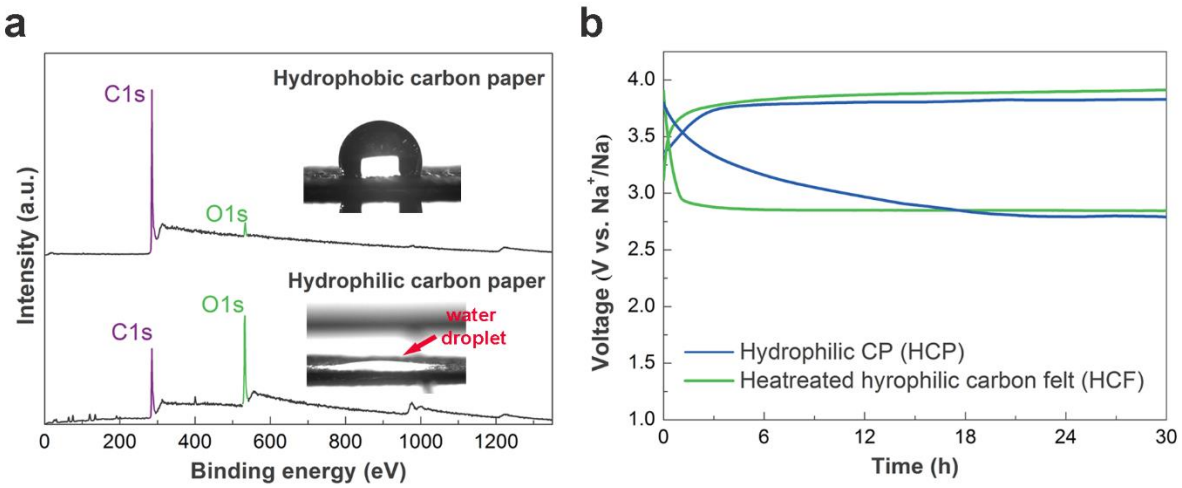

Figure 24. Characterization of both neutral hydrophilic carbon paper (HCP) and hydrophobic carbon paper and the surface wettability effects in saltwater battery. (a) XPS wide-scan spectra of hydrophobic (top) and hydrophilic (bottom) CP (HCP). The insets show wetting behavior of the paper, respectively. (b) Galvanostatic discharge curves in Na|saltwater (1 M) with different carbon paper used as current collector, respectively.

Graphene oxide coated carbon paper (GOCP), to solve the problem, was employed to change the surface property of hydrophobic carbon paper. The graphene oxide (GO) bears hydroxyl and epoxide functional groups on their basal planes, in addition to carbonyl and carboxyl groups located at the sheet edges. Thus, the GO has quite hydrophilic properties [85]. High resolution SEM analysis was observed to confirm the existence of the GO on carbon paper as shown in Fig. 25b. Unlike hydrophobic carbon paper, the high resolution SEM image exhibits carbon fibers and graphene oxides, which looks like a web shown among fibers (Fig. 25 a, b). Inset magnifying a graphene oxide coated fiber was revealed more crumpled fiber than bare carbon paper. In addition, the Raman spectra is in good agreement with D and G bands of graphene D at 1351 cm^{-1} , G at 1561 cm^{-1} and 2D at 2684 cm^{-1} (refs. 86,87,88) and the I_D/I_G ratio give more information about graphene coated carbon paper have I_D/I_G ratio of around ~1 (Fig. 25f). XPS wide-scan spectrum of hydrophobic CP and GOCP (Fig. 25g) is similar to the results in Fig. 7c. Since GOCP has a higher O/C ratio than pristine, it is expected that the hydrophilicity of the surface would be enhanced. The C1s spectrum in Fig. 8h show three types of

carbon bonds C=C, C-O-C and carbonyl (C=O) at 284.1, 285.8 and ~ 288 eV, respectively (Fig. 25h) [86,87,88]. After coating GO on the carbon paper, the C-O bonds appeared at around 286 eV. The measurement of the contact angle indicates that GO makes the surface of carbon paper hydrophilic as shown in Fig. 25a and b. According to these results, GOCP can be substituted for HCP. Electrochemical performance was investigated to check whether the GOCP can be used as a positive current collector in Fig. 26. The charge and discharge voltage profiles were performed with Na| 1M saltwater using various types of CPs (GOCP, hydrophobic CP, HCP). Against expectations, the cell of GOCP shows lower discharge voltage (~2.5 V) than others. The poor voltage efficiency is estimated to low electrical conductivity of GOCP as shown in Fig. 27. Many researchers, therefore, have tried to improve it, for example, by doing Nitrogen [80,89,90]. In conclusion, GOCP is inappropriate for a cathodic current collector in saltwater battery although it has good wettability.

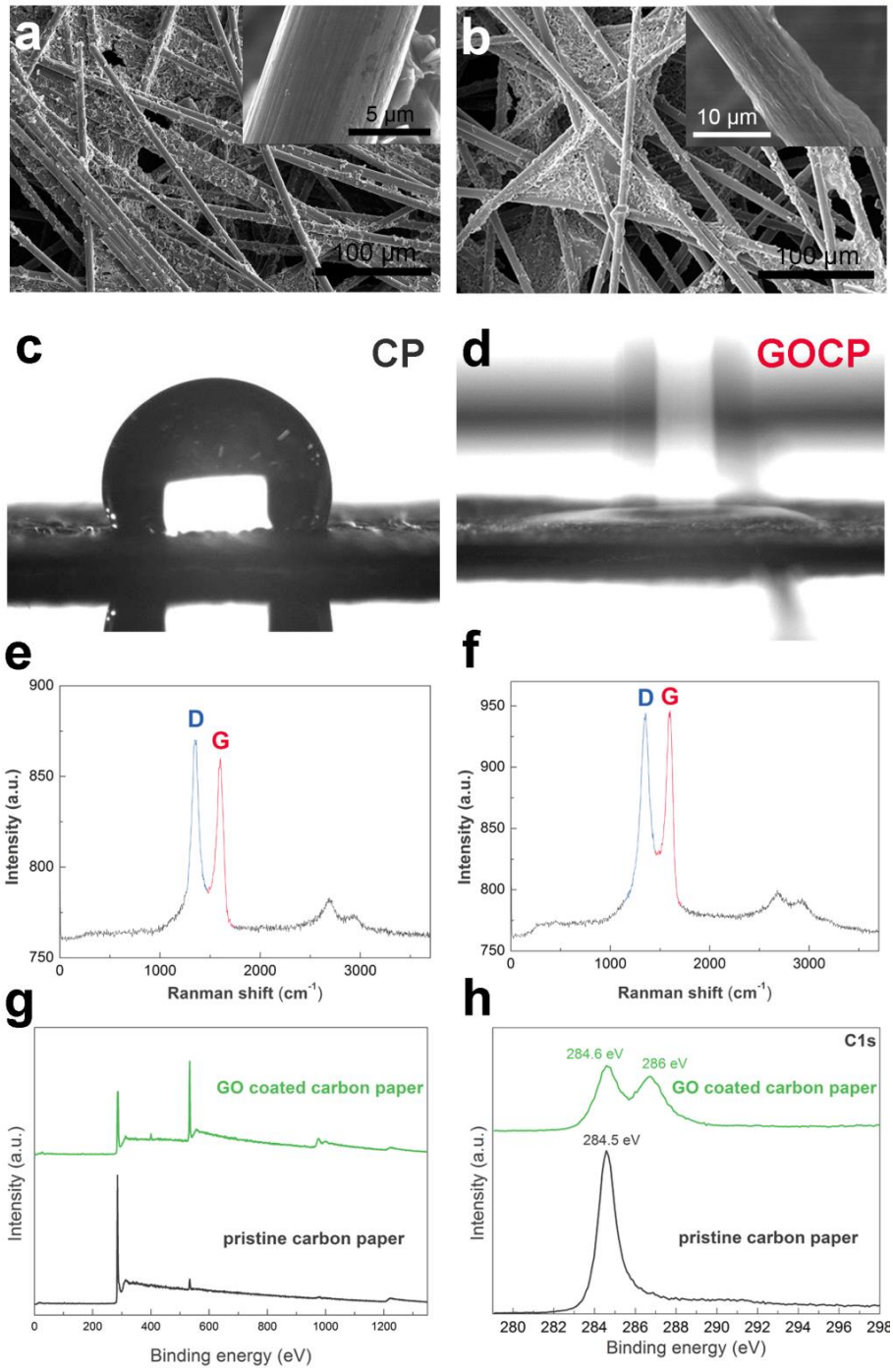

Figure 25. Characterization of hydrophobic carbon paper (CP) and graphene oxide-coated carbon paper (GOCP). SEM images of (a) hydrophilic carbon paper (HCP) and (b) GOCP used as current collector. The inset shows an enlarged image of a strand of the paper, respectively. Wetting behavior of (c) CP and (d) GOCP. Raman spectra of (e) CP and (f) GOCP, which show two distinct peaks at ~1350 and ~1562 cm^{-1} corresponding to D and G bands, respectively. (g) XPS wide-scan spectra of CP (bottom) and GOCP (top). (h) XPS narrow-scan spectra of the C 1s peak for CP and GOCP.

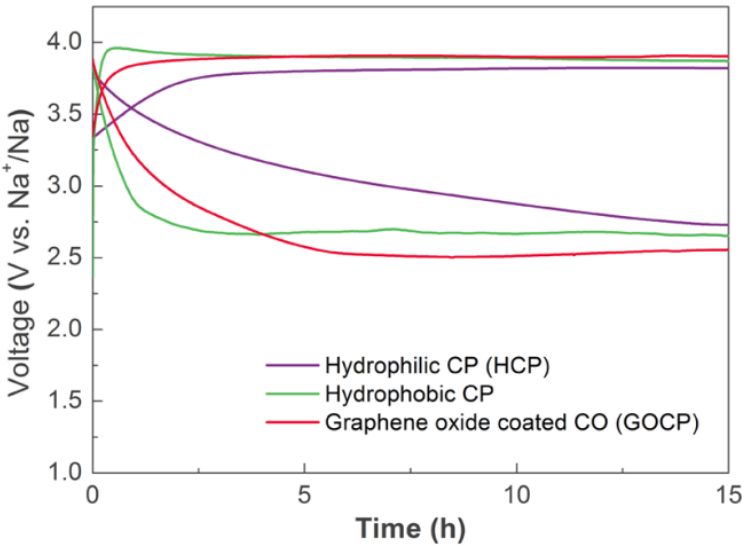

Figure 26. Electrochemical performances with various type of CP. First cycles of galvanostatic charge and discharge curves in Na|saltwater (1 M) at a current rate of 0.025 mA/cm^2 with different types of CPs.

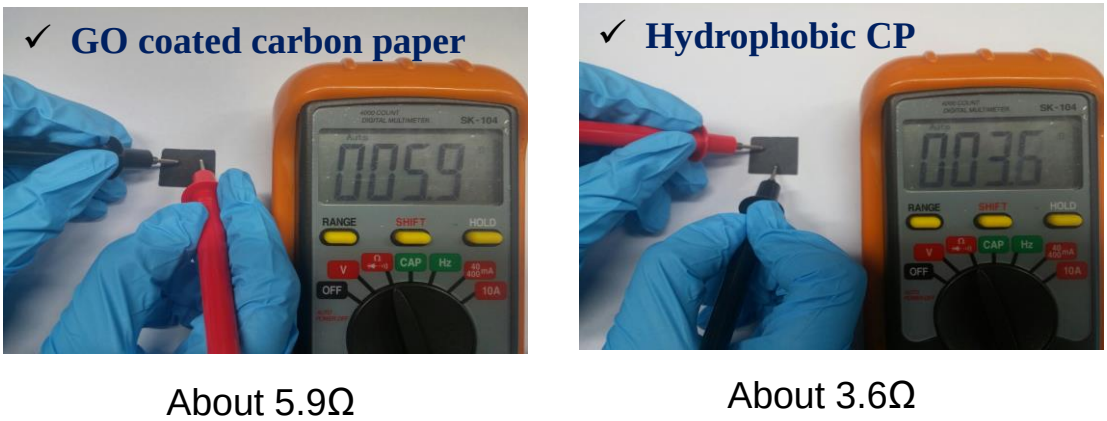

Figure 27. Electrical resistance-measurement for GOCP (left) and CP (right).

Neutral HCP has functionalized well as a cathodic current collector. It has a highly wetted surface and is thin enough to be attached easily to NASICON so that there is no gap between them. However, carbon paper is somewhat brittle so that it may have trouble in scale-up.

Carbon felt (CF) is a new candidate as a positive current collector, which has been commonly used in redox-flow batteries (RFB). It has been reported that CF has 3-dimentional networks and provides numerous electrochemical reaction sites. CF would be expected to be available for scale-up owing to its flexibility [80]. Moreover, the cost per area is more inexpensive than carbon paper, for example, those of CP and CF are 73 ₩/cm^2 and 40 ₩/cm^2, respectively. To study the possibility of using CF, some analysis including electrochemical tests were conducted. Commonly, CF has a hydrophobic surface resulting from small amounts of oxygen functional groups. So to resolve the issue, it has been used with surface modifications such as thermal treatment, coating catalyst and so on [80,81,91,92,93]. Thermal treatment is the easiest method to make a hydrophilic surface. When CF is heat-treat in the air, oxygen remains on the surface, as oxygen functional groups (e.g. CO), and the CF is oxidized [92]. Therefore, the thermal activation is employed to improve the wetted surface. In this work, the CF was heat-treated under 500 ^oC and 2 hours in the air. In order to examine the surface morphology of heat-treated and untreated CF, SEM and contact angle measurements were used, as shown in Fig. 28a. Unlike CP, the carbon fibers of CF, seems flexible. A certain change after thermal activation did not appear in the SEM image. However, the result of the contact angle measurement shows that the surface wettability after heat-treatment increased dramatically (Fig. 28a). The results of electrochemical test also indicated that electrochemical performance of the saltwater battery was improved by using heat-treated hydrophilic CF (HCF) (Fig. 28b). First, the cells with different CF (HCF and heat-untreated CF) were charged and discharged for 5 hours, respectively, at a current rate of 0.025 mA/cm^2 so as to investigate the effect of thermal activation. The cell using untreated CF (pristine CF) showed high overpotential at first charge, but it recovered after that. The reason for that is likely to be poor activation polarization in accordance with the hydrophobic surface [83,91]. The further investigation on availability of HCF was conducted with charge and discharge for 30 hours at the same current rate above (Fig. 28c). Although HCF electrode cell exhibited similar discharge voltage to that of HCP, the discharge voltage behaviors are quite different and the HCF cell reached the point first. It is probably that which side reactions happened at the early discharge process of HCP cell [94]. This result indicated that activity and stability of HCF electrode were better than that of HCP. Thus, HCF has been suitable to a cathodic current collector and it was employed in improving cell performances with oxygen evolution reaction (OER) and/or oxygen reduction reaction (ORR) catalysts.

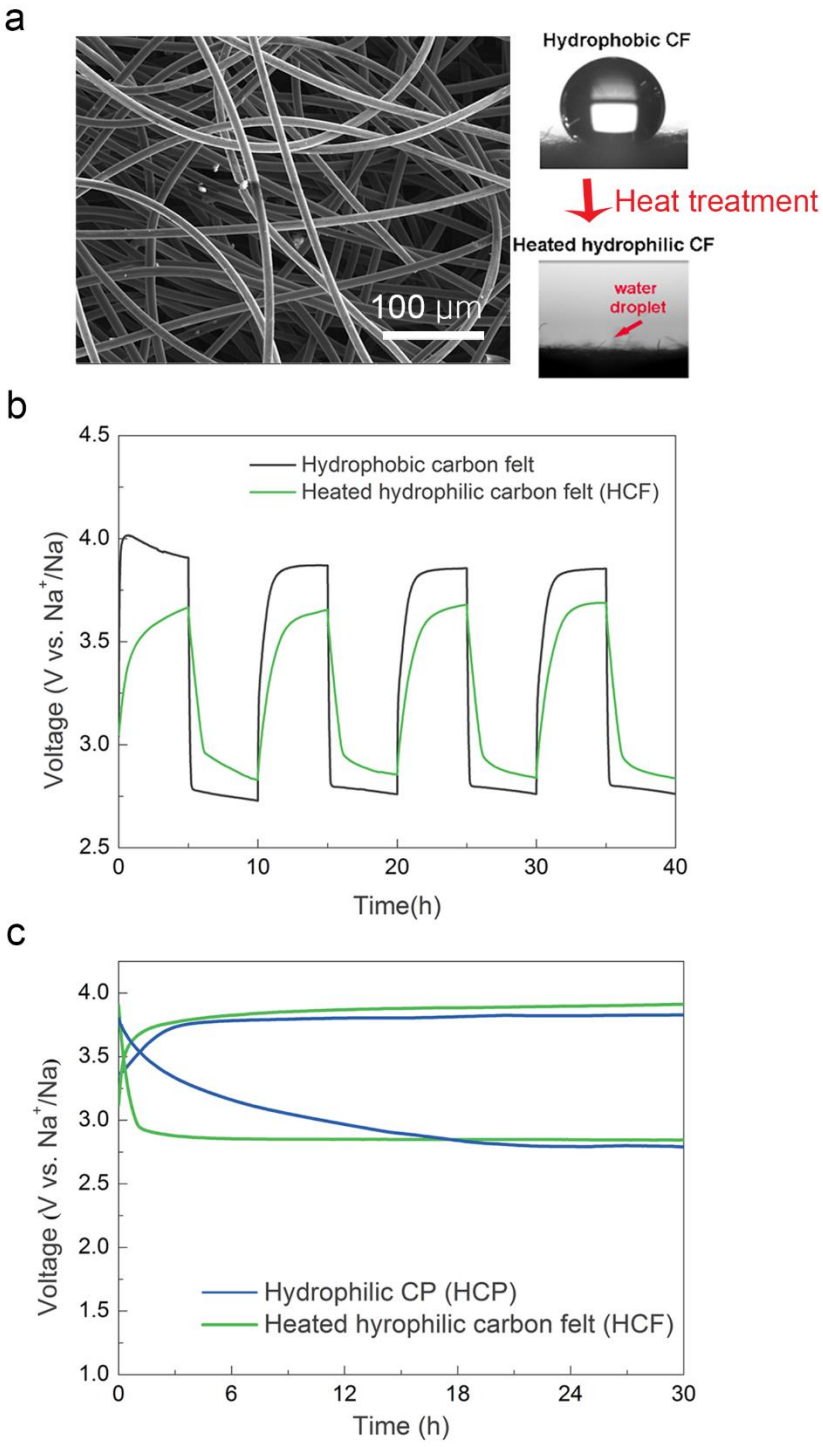

Figure 28. Investigation of heated carbon felt (HCF) as a positive electrode. (a) A SEM image of heated hydrophilic carbon felt (HCF) and its contact angle images before and after heat-treatment under 500 ^{o}C and 2 hours. Electrochemical tests of cells using HCF, comparing to (b) pristine carbon felt and (c) hydrophilic carbon paper at the currents of 0.025 mA/cm^2.

3.2. Mechanism.

3.2.1. Reaction mechanism.

The catholyte of saltwater battery is copiously composed of salt (NaCl) and water. So, when the saltwater battery is charged, the oxygen evolution reaction (OER) and chlorine evolution reaction (CER) could occur as follows (Fig. 29a, b) [42,43,44].

Oxygen evolution reaction (OER) :

$$H_2O(l) + 2NaCl(aq) \rightarrow 2Na(s) + (1/2)O_2(g) + 2HCl(aq)\ , \qquad E^o = 3.94\ V\ \textit{vs.}\ SHE \qquad (1)$$

Chlorine evolution reaction (CER) :

$$2NaCl(aq) \rightarrow Cl_2(g) + 2\ Na(s)\ , \qquad E^o = 4.07\ V\ \textit{vs.}\ SHE \qquad (2)$$

These thermodynamic equations usually represented standard potential (E^o), derived from standard state, which refers to 25 ^oC and active species of 1 M (concentration) or 1 atm (partial pressure) corresponding to activity of 1 (refs. 95,96). However, cells operate non-standard condition in practice and the cell potentials will be changed, following the Nernst equation [95,96]. The saltwater battery operated at room temperature, but the active species are not consistent with the standard condition. Most saltwater (from low to high concentration) is generally a neutral solution of pH6~pH7. On the contrary, the standard potential of OER refers to pH 0 of 1 M protons in solution. Accordingly, the cell potential of OER is changed as a function of pH, unlike CER. This relation between potential and pH are well known as pourbaix diagram that analyze the electrochemical window of aqueous solution (Fig. 29c) [97]. The graph exhibits upper slope of OER and oxygen reduction reaction (ORR) and lower slop of hydrogen evolution reaction (HER). With respect to the pourbaix diagram, OER in a saltwater battery is changed as below (Fig. 29b). :

$$\text{Cathode} : (1/2)H_2O(l) \rightarrow (1/4)O_2(g) + H^+(aq) + e, \qquad E=0.81\ V\ vs.\ SHE\ (pH\ 7) \qquad (3)$$

$$\text{Anode} : Na^+(aq) + e \rightarrow Na(s), \qquad E=-2.71\ V\ vs.\ SHE \qquad (4)$$

$$\text{Overall} : NaCl(aq) + (1/2)H_2O(l) \rightarrow Na(s) + (1/4)O_2(g) + HCl(aq), \qquad E=3.53V \qquad (5)$$

Therefore, the predicted potentials for OER and CER is 3.53 V and 4.07 V, respectively.

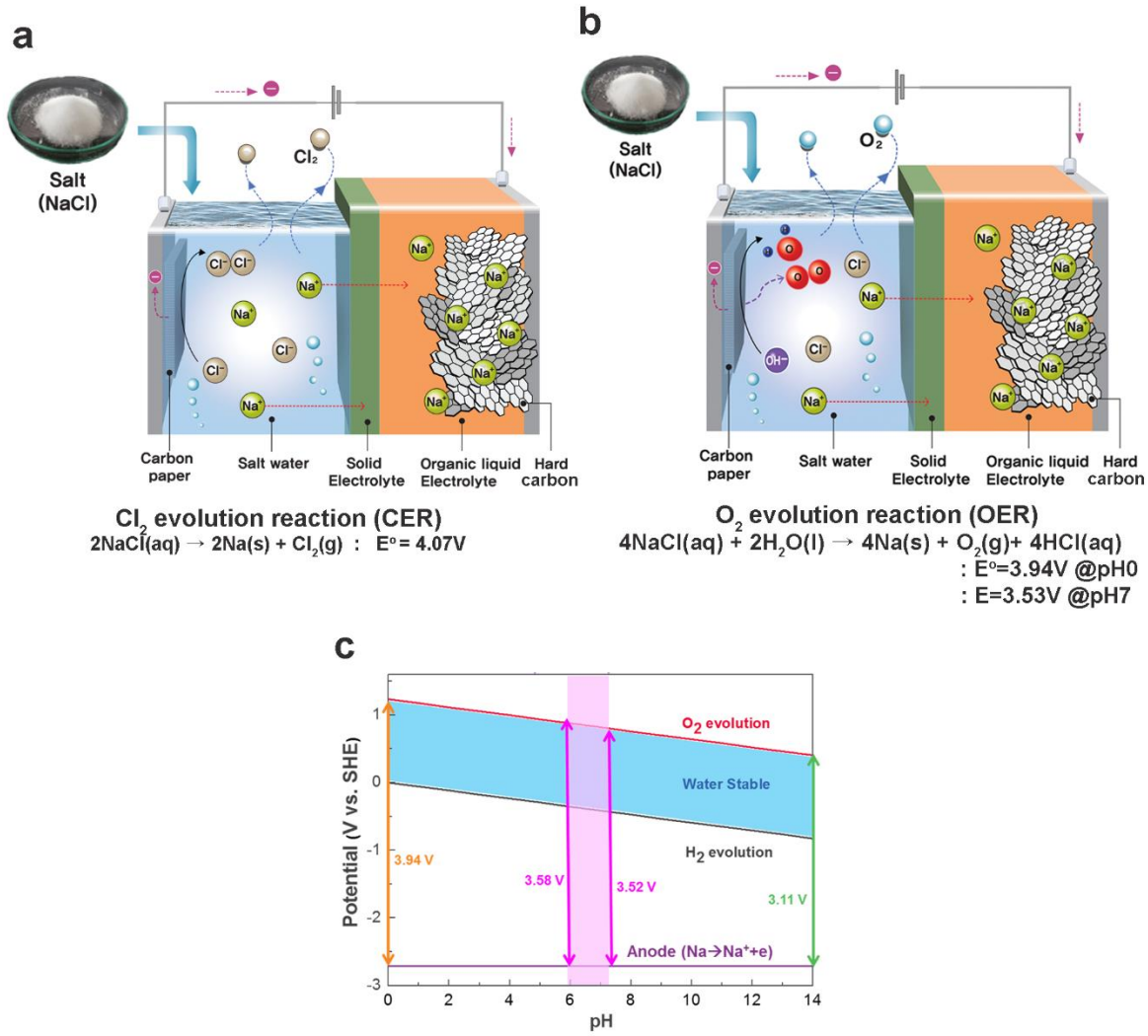

Figure 29. Theoretical reactions during charge process. (a) Chlorine evolution reaction (CER) (b) Oxygen evolution reaction (OER) (c) Pourbaix diagram of water showing the pH range for saltwater. The blue region indicates H_2O-stable potential window (0-1.23 V at pH 0). It should be noted that the redox potentials of ORR and OER vary with the pH.

As shown in Fig. 30a, a saltwater battery, composed of Na|1 M saltwater, was charged at around 3.8 V. Since the measured charge voltage was lower than the theoretical potential of CER (4.07 V), the main electrochemical reaction during charge would be OER rather than CER. And the overpotential during charging is around 0.31 V. Previous works in seawater batteries showed the evidence of CER during the charging, as the concentration of Cl^- decreased with charging time. In this study we also observed that the concentration of Cl^- decreased monotonically with increasing charging time for the battery with 0.4 M saltwater, which is comparable to the NaCl concentration in seawater (Fig. 30b) [44]. Parallel to the oxidation of saltwater by OER, Na^+ dissolved in the catholyte are transferred to the anode side through the NASICON and then reduced to Na metal. After charging over 200 hours at a current rate of 0.1 mA/cm^2, extracted Na metal from saltwater was observed and identified from the EDS data. Dark gray color deposition indicates Na metal extracted from NaCl(aq.) (Fig. 30c, d). The EDS results also demonstrate the extraction of Na from saltwater during charging (Fig. 30e, f).

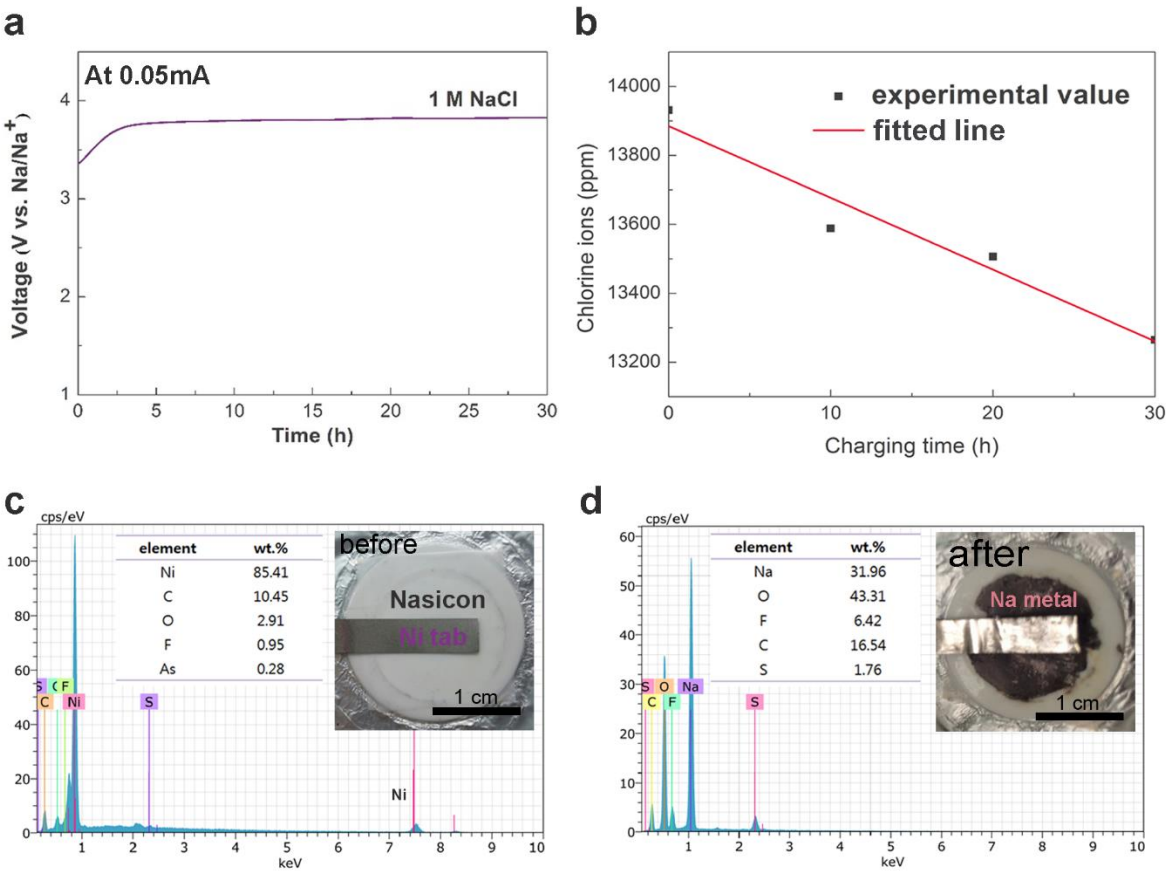

Figure 30. Charge process in saltwater battery. (a) Galvanostatic charge voltage curve corresponding to Na|saltwater (1 M) half-cell. (b) Variation of the concentration of Cl- ions in 0.4 M saltwater over 30 hours of charging. Digital pictures and EDS result for anode side (c) before and (d) after charging over 200 hours at a current rate of 0.1 mA/cm^2, showing harvested Na from saltwater.

To further investigate the occurrence of CER and OER in saltwater during charge, we measured the cyclic voltammogram (CV) of a 1 M NaCl (*aq*) using a three-electrode half-cell at a scan rate of 10 mV/s and compared it to that using 1 M Na_2SO_4 (*aq*). The latter has no Cl^- ions, therefore no CER would occur [98]. As shown in Fig. 31, within a potential window of 0–1.1 V *vs.* SHE (2.7–3.8 V *vs.* Na^+/Na), 1 M NaCl displayed a couple of redox current signals with a voltage difference, which could be assigned to OER and ORR in the anodic and cathodic directions, respectively. On the other hand, the CV curve within a potential window of 0–1.4 V *vs.* SHE (2.7–4.1 V *vs.* Na^+/Na, green curve in Fig. 31) reveals significantly larger anodic currents and an additional reduction peak (at approximately 1.15 V *vs.* SHE) in the cathodic scan. The increased current appears to be a result of CER [99] in addition to OER, and the reduction peak corresponds to CRR [98,100]. Based on the CV results and the galvanostatic charge-discharge voltage profile, we consider the saltwater battery charges mainly by OER due to the electrolysis of the saltwater at the cathode side, although CER cannot be completely ruled out. The dominance of OER is also corroborated by the CV result of 1 M Na_2SO_4 (Fig. 31, dashed line), which is very close to that of 1 M NaCl.

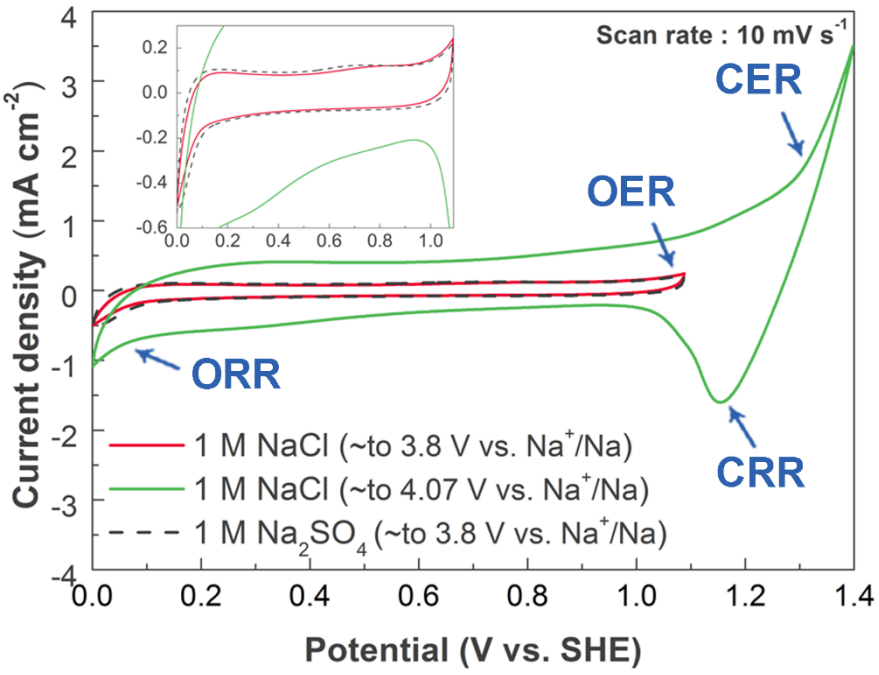

Figure 31. Cyclic voltammograms of 1 M saltwater and 1 M Na_2SO_4 aqueous solution at a scan rate of 10 mV/s. An enlarged portion (inset) shows no notable difference between two sets of CV curves.

During discharge of the saltwater battery, Na is oxidized to Na^+ ions, moving to the catholyte and two possible reactions may occur as below (Equation 6, 8). The reactions relate to pH since protons and hydroxide ions involve the reactions. And theoretical discharge potentials are also changed depending on pH and can be changed to 3.52 V and 2.29 V, respectively (Equation 7, 9).

Oxygen reduction reaction (ORR) :

$$Na(s) + (1/2)H_2O(l) + (1/4)O_2(g) \rightarrow NaOH(aq), \quad E^o = 3.11 \text{ V vs. SHE} \tag{6}$$

$$E = 3.52 \text{ V vs. SHE (pH 7)} \tag{7}$$

Hydrogen evolution reaction (HER) :

$$Na(s) + H_2O(l) \rightarrow NaOH(aq) + (1/2)H_2(g), \quad E^o = 1.88 \text{ V vs. SHE} \tag{8}$$

$$E = 2.29 \text{ V vs. SHE (pH 7)} \tag{9}$$

There were enough oxygen gases, dissolved in saltwater, to cover the discharge reaction of ORR. If the oxygen gases decrease, it would be supplied from air and saltwater would keep the concentration of dissolved gases. In other words, ORR may occur dominantly under discharge as shown in Fig. 32a. When discharging a saltwater battery of Na|1 M saltwater, discharge voltage plateau was 2.8 V as shown Fig. 32b and it was expected owing to reacting with H_2O and O_2 to form NaOH discharge product with oxygen reduction reaction (ORR). The same discharge mechanism was demonstrated in a seawater battery. Fig. 31b (inset) shows that the prototype-cell, constructed with Na|saltwater (1 M), was lighting a bulb with discharge.

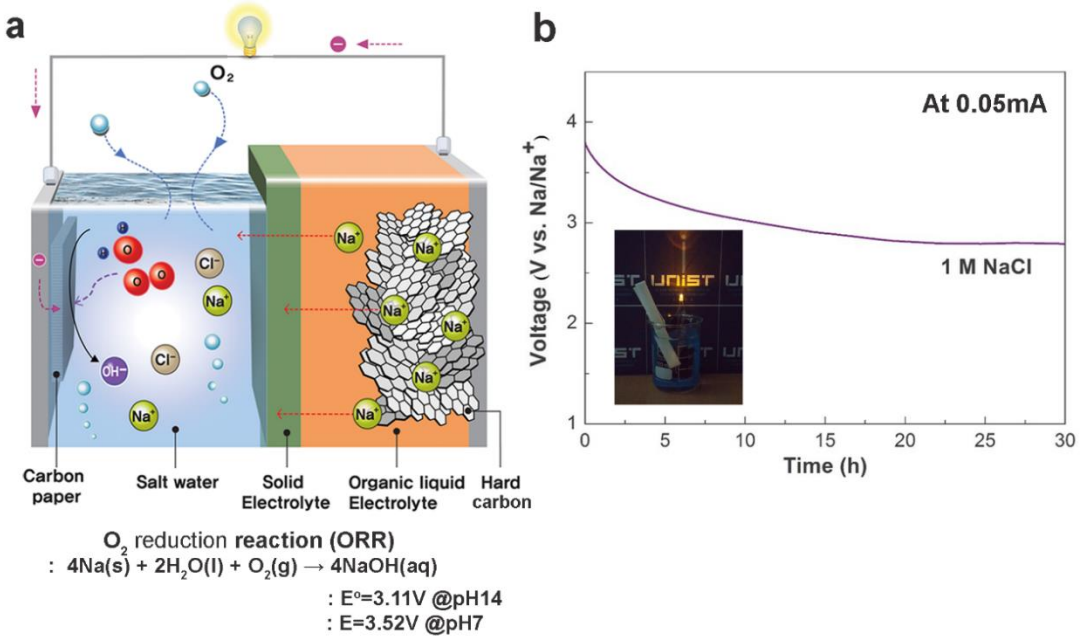

Figure 32. Discharge process in saltwater battery. (a) Schematic diagram presenting discharging. (b) Galvanostatic discharge voltage curve with Na|saltwater (1 M) half-cell. Inset, photograph of saltwater battery lighting an LED bulb.

3.2.2. Influence of salt concentration.

To confirm influence of the concentration of NaCl for the saltwater battery, the voltammetric behavior and galvanostatic electrochemical tests were studied with 5 M NaCl under the same conditions as above. In Fig. 33a, the CV shape of 5 M saltwater also showed no peak of CRR and thus, OER happened mainly during charge process though increase in NaCl concentration. Investigation with differential electrochemical mass spectroscopy (DEMS) is also anticipated to demonstrate the reaction mechanism under high concentration [99]. There is charge and discharge profiles of Na|saltwater (1 and 5 M) half-cells as shown Fig. 33b. The charge voltage plateau (~3.7 V) of 5 M NaCl was lower than that (~3.8 V) of 1 M NaCl and the discharge voltages were ~2.6 V (5 M) and ~2.8 V (1 M), respectively. This meant the charge and discharge potentials were decreased as increasing salt concentration and it corresponded to thermodynamic values, calculated with the Nernst equation (Fig. 33c). The reaction quotient in the Nernst equation varies with active species, resulting in changing cell potential [101].

To investigate the influence of the concentration of NaCl for the saltwater battery, various concentrations (0.4, 1, 3 and 5 M) of NaCl aqueous solutions (catholyte) were prepared and tested in half cells. The same result as galvanostatic electrochemical test was turned out. When concentration of NaCl was increased, lower charge voltage was observed as shown Fig. 34a. This could be attributed to the increase in the ionic-conductivity in higher salt concentration (Fig. 34b) as well as variation of reaction quotient. This indicates that the kinetics derived from concentration polarization of 5 M saltwater is faster than the lower concentration solution. Accordingly, the high concentration solution had lower resistance than low concentration solution at interface between NASICON and saltwater [102]. Thus, Na-ions in the high concentration solution can transport easily through NASICON.

The lower discharge voltage appeared as the concentration of NaCl was increased (Fig. 34a), although high salt concentration had high-ion conductivities. This was probably attributed to kinetics at the interface between NASICON and saltwater as shown in Fig. 34c. On discharge, Na is oxidized to Na^+ ions and the electron transferred to positive current collector, resulting in negative charge of saltwater (Fig. 34d). Na^+ ions accordingly diffused through NASICON from anode to cathode to maintain charge balance. At this point, the Na^+ ions might meet higher resistance at the interface under 5 M saltwater that 1 M. Tendency of concentration influence was shown in this research but the further studies for the reason and optimum concentration will be required.

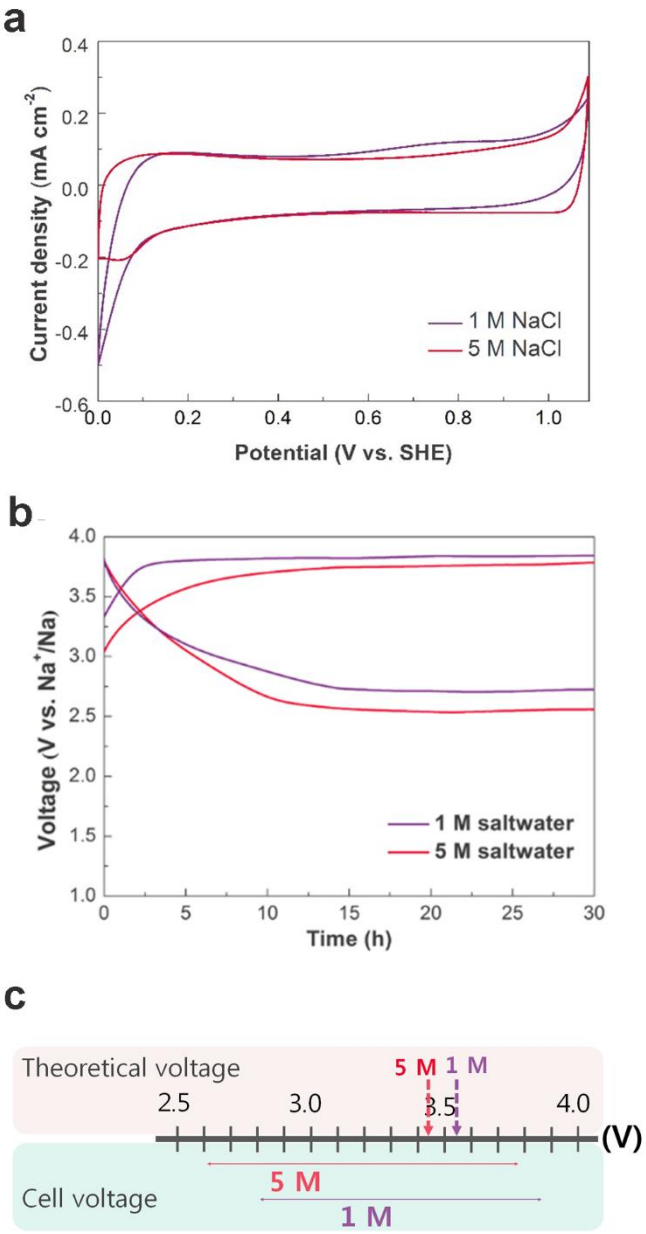

Figure 33. Influence of salt concentration. (a) Cyclic voltammograms of 1 and 5 M NaCl aqueous solution at the range of cell-operation. (b) Galvanostatic charge voltage curve corresponding to Na|saltwater (1 M and 5 M) half-cell, separately, at a current rate of 0.025 mA/cm^2. (c) Comparison of theoretical cell voltage and experimental voltage as a function of salt concentration.

a

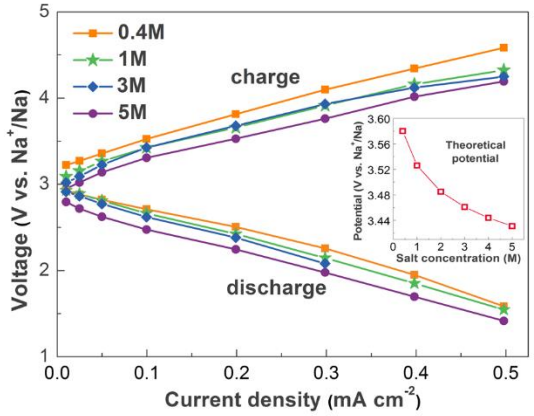

b

solution	conductivity (mS/cm)
DI water	10^{-5}
0.4 M saltwater	42
1 M saltwater	89.7
3 M saltwater	196.4
5 M saltwater	>199

c

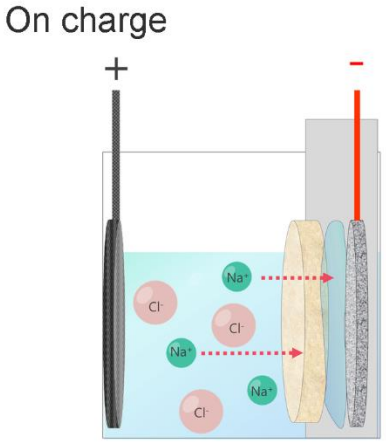

d

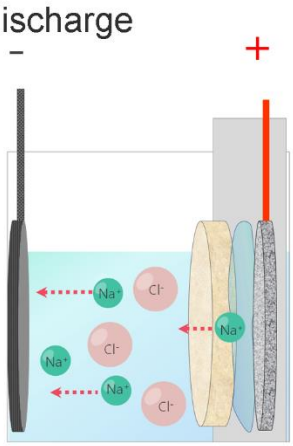

Figure 34. Concentration polarization. (a) Polarization plots with respect to salt concentration, including 0.4 (square), 1 (star), 3 (diamond) and 5 M (circle) at charge and discharge with different current rates of 0.01, 0.025, 0.05, 0.1, 0.2, 0.3, 0.4, and 0.5 mA/cm^2. (b) Measured ion conductivities of the solutions. Schematic diagram of concentration polarization around interface between NASICON and saltwater during (c) charge and (d) discharge.

3.2.3. Calculation of theoretical energy density.

In the case of 5 M saltwater, the theoretical potential of the following redox reactions in the cathode side is calculated to be 3.43 V *vs.* Na^+/Na according to the Nernst equation.

$$Na\ (s) + ½\ H_2O\ (l) + ¼\ O_2\ (g) \leftrightarrow NaOH\ (aq);\ E^0=3.43\ V\ vs.\ Na^+/Na\ (pH=7) \quad (7)$$

The theoretical gravimetric energy density was calculated using the following equation

$$\text{Theoretical energy density (mass)} = \frac{E_{rev} \cdot Q(5M\ NaCl)}{m_{anode}+m_{cathode}} = 368\ \text{Wh/kg} \quad (10)$$

The theoretical redox potential E_{rev} is 3.43 V and Q is the quantity of electrical charge for 5 mole electrons generated from 1 L NaCl aqueous solution at 5 M ($Q = 96485\ \text{C/mol} \times 5\ mole/L \times \frac{1\ hr}{3600\ sec}$). The mass of 1L saltwater is derived from its density ($\rho_{5M,\ saltwater}$ = 1.241 g/mL) [103]. Oxygen is assumed to be completely dissolved in the saltwater, and its mass is regarded as ¼ of 5 mole according to reaction (Equation 7) [104]. Since Na can be fully provided from the saltwater during charging, the mass of the anode is not considered in this calculation. Therefore, the total mass of the anode and cathode is 1.241 kg, resulting in a theoretical energy density of 368 Wh/kg. Likewise, for a battery with 6 M saltwater, the theoretical energy density is calculated to be 423 Wh/kg, based on the theoretical redox potential (3.42 V *vs.* Na^+/Na) and density ($\rho_{6M,\ saltwater}$ = 1.295 g/mL).

3.3. Electrochemical performances.

The electrochemical performance of the Na-metal-free saltwater battery is first examined through half-cells: an anode half-cell with hard carbon electrode and a cathode half-cell with saltwater. As a representative sodium-intercalation material, hard carbon exhibits high reversible capacity (250–300 mAh/g) and low sodium-ion-insertion potential (<1.0 V *vs.* Na^+/Na) [47,105]. Hard carbon as the negative electrode can thus avoid poor reversibility (cyclability) stemming from the dendritic growth of Na metal during cell operation. Theoretically, the energy density of saltwater batteries is dependent on the concentration of NaCl (catholyte) and the capacity of anode. Considering the maximum solubility of NaCl in water (6 M at 25 °C) and the stability of the NaCl solution at room temperature, we assembled a half-cell saltwater battery with Na metal and 5 M saltwater catholyte, whose theoretical energy density was calculated to be 368 Wh/kg (for details see section of energy density). For the anode, we evaluated the electrochemical properties of a hard carbon electrode using a 2032 coin-type half-cell (Na|hard carbon). The galvanostatic charge-discharge profiles at the current rate of 0.025 mA/cm^2 (approximately 26 mA/$g_{\text{hard carbon}}$) are shown in Fig. 35. The hard carbon electrode delivered initial discharge (sodiation) and charge (desodiation) capacities of 557 and 370 mAh/g, respectively, with an irreversible capacity decay of 187 mAh/g during the first cycle. The low initial Coulombic efficiency (66 %) could be ascribed to the formation of the solid-electrolyte interphase (SEI) on the hard carbon surface and the trapping of a small amount of Na^+ in the hard carbon [106]. After five cycles, the hard carbon electrode displayed a reversible capacity of 350 mAh/g.

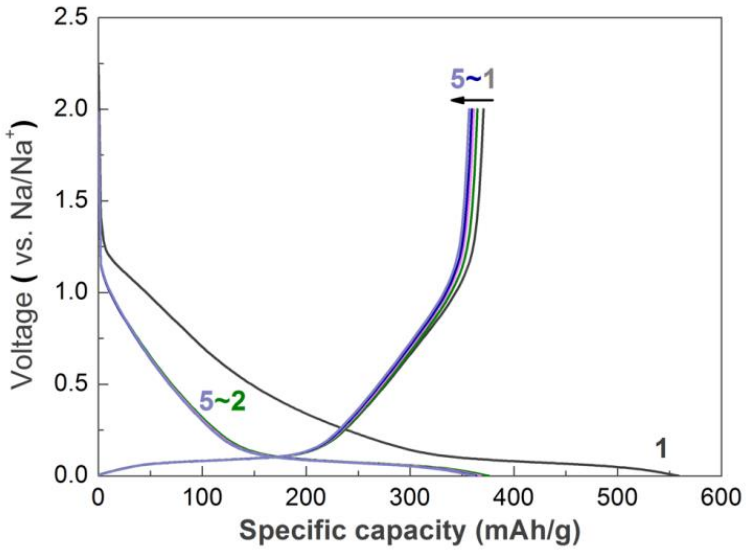

Figure 35. Electrochemical performance of the 2032 coin-type half-cell (Na|hard carbon). The galvanostatic charge and discharge voltage profiles at a current rate of 0.025 mA/cm^2 for 5 cycles show the reversible capacity of 350 mAh/g.

Fig. 36a exhibits the galvanostatic charge and discharge curves of the cathode and anode half-cells. The cathode half-cell (Na|5 M saltwater) showed charge and discharge voltage plateaus at 3.76 V and 2.56 V, respectively. In the case of the anode half-cell, the charge-discharge profiles were based on the 5th charge-discharge profiles of (Na|hard carbon) half-cell.

Next, we constructed the full-cell saltwater battery (hard carbon|5 M saltwater) and investigated its performance. The full-cell saltwater battery was tested at a current rate of 0.025 mA/cm^2 with a capacity cut-off condition of 300 mAh/$g_{\text{hard carbon}}$ upon charging, and a voltage cut-off condition of 0.5 V upon discharging (Fig. 36b). At the first cycle, the saltwater battery displayed a considerably low discharge capacity of 46 mAh/g (initial Coulombic efficiency 15 %), which was attributed mainly to the formation of the SEI layer during charging (sodiation). It was assumed that during the first charging, most of the input charge (300 mAh/$g_{\text{hard carbon}}$) was consumed to form the SEI on the surface of the hard carbon anode. Indeed, the first charge voltage profile of the full-cell corresponded to the sloping region (1.2 V–0.1 V) of the initial discharge voltage profile of the anode half-cell (Na|hard carbon). Such a sloping region has been recognised as caused by SEI formation, as well as Na^+-insertion within the graphene layers of hard carbon [106]. As the cycling continued, the discharge capacity steadily increased and the charge-discharge voltage profiles became saturated at the 7th cycle. Fig. 36b exhibits the 7th charge-discharge voltage profile, which was close to the voltage profiles predicted from the two half-cell voltage profiles in Fig. 36a (orange curves). The average charge and discharge voltages of the full-cell were 2.78 V and 2.45 V, respectively.

To examine the Na^+ insertion from the saltwater catholyte into the hard carbon anode, the anode surface of the full-cell disassembled after the 8th charge process was examined by SEM with EDS, and XPS. The EDS mapping data (Fig. 37a) revealed an increased amount of Na element with uniform distribution after cycling compared to the pristine electrode, which only showed a weak Na signal from the remnant $NaCF_3SO_3$ salt. Result of XPS (Fig. 37b) measurement indicated the intensity of Na 1s considerably increased after charge. Therefore, it means that the Na-ion from saltwater is inserted to hard carbon.

Fig. 36d shows the cycling performance of the full-cell saltwater battery at a current density of 0.025 mA/cm^2 over 50 cycles. Although the discharge capacity was initially quite low, it increased with cycling number and reached the saturation level of 294 mAh/g by the 7th cycle, reaching a high Coulombic efficiency of 98.2 %. The full-cell displayed excellent cycling stability without significant capacity fading during 50 cycles. The discharge capacity after the 7th cycle was between 294 and 296 mAh/g and the Coulombic efficiency was maintained at 98 % over 50 cycles. Even after 50 cycles, no noticeable XRD peak shift was observed for the NASICON pellet (Fig. 38), indicating its stability.

This behavior is different from that observed in conventional rechargeable batteries, where the battery performance is generally tested with *voltage cut-off* conditions at constant currents upon both

charge and discharge. In contrast, our full-cell saltwater batteries were examined with a *capacity cut-off* condition of 300 mAh/$g_{\text{hard carbon}}$, which is lower than the estimated reversible capacity of the hard carbon electrode upon charge. This controlled testing could avoid unwanted Na plating (dendritic growth) on the anode surface during the charge of the full-cell, and consequently allow more stable cycling performance.

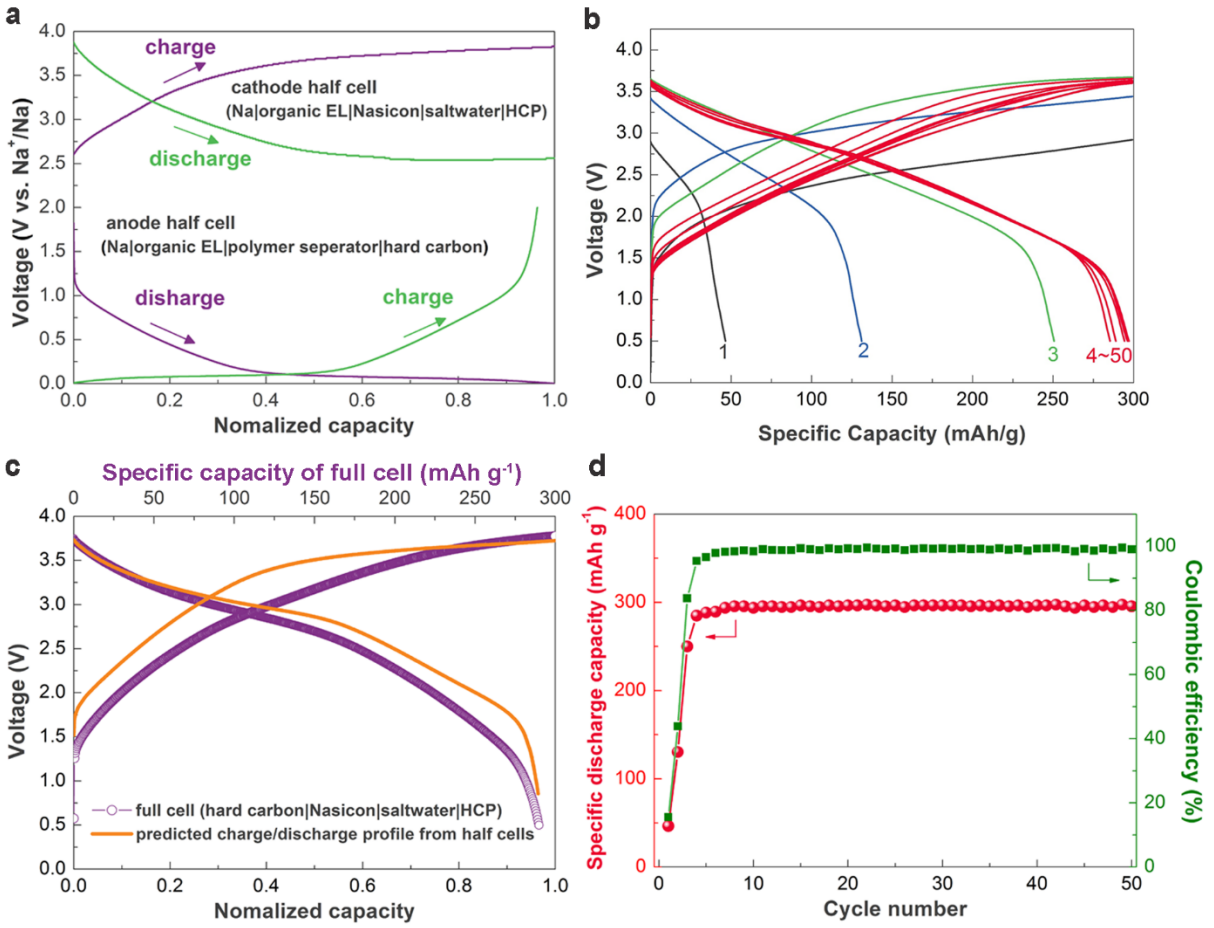

Figure 36. Electrochemical performance of the rechargeable saltwater battery. (a) Galvanostatic charge and discharge voltage profiles of the cathode and anode half-cells at a current rate of 0.025 mA/cm^2 (b) Galvanostatic charge and discharge voltage curves of the full-cell (hard carbon|5 M saltwater) for 50 cycles at a current rate of 0.025 mA/cm^2. (c) Purple: The 7th charge and discharge curves of the full-cell (hard carbon|5M saltwater) at a current rate of 0.025 mA/cm^2. The orange curves depict the prediction from the two half-cell results in panel (a). (d) Cycling performance of the full-cell over 50 cycles.

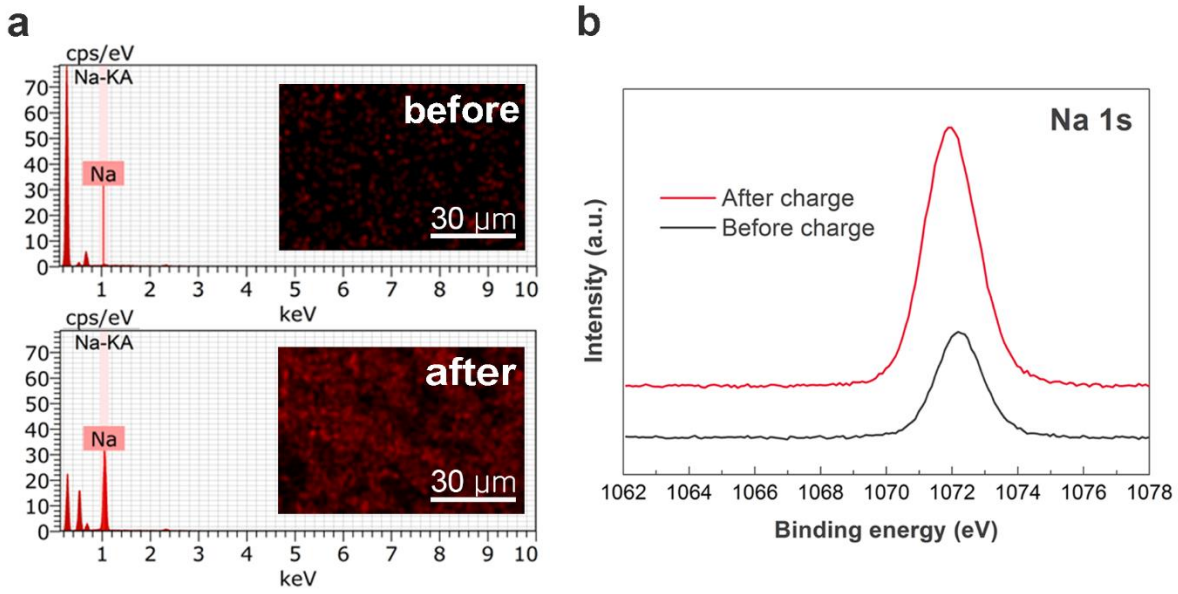

Figure 37. Characterization of hard carbon after and before charge. (a) EDS mapping results of the hard carbon anode before cycling, and after the 8th charge process. (b) XPS of hard carbon before and after charge shows high-resolution XPS core level spectra of Na 1s.

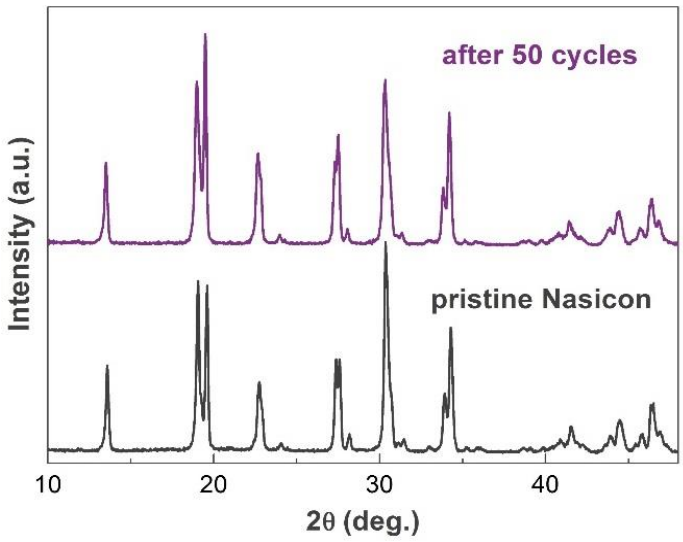

Figure 38. XRD patterns of the pristine NASICON and after 50 cycles. Although the peak intensities changed slightly, no noticeable peak shift was observed between the two spectra, revealing the stability of NASICON in saltwater during cycling.

3.3. Catalysts.

The reaction rates, in a saltwater battery of oxygen evolution during charge and oxygen reduction during discharge, have a great effect on determining the electrochemical performance. For example, the potential gap occurs between a theoretical and experimental reaction, known as overpential, and the voltage efficiency of a cell becomes lower as higher overpotential. Using catalysts is a significantly attractive solution in this challenge. Catalysts are well known to diminish the activation energy and make a specific reaction fast, resulting in increasing reaction kinetics with low overpotentials. There are some requirements such as good electrochemical activity, good electrical conductivity and stability in keeping catalytic activity, to fulfill high cell performance. The condition of acatalyst coated on an electrode (e.g. dispersion, agglomeration) and durability on an electrode are also significant requirements [107].

As a first step to explore the feasibility of a catalyst in the saltwater battery, Pt/C (50 wt%) and Vulcan XC72R (that was used to support Pt) were coated on the heated carbon felt (HCF), which was flexible and hydrophilic. Platinum (Pt) catalyzed carbon material (Pt/C) generally exhibits excellent performance for OER and ORR and thus, the catalyst has been applied to fuel cells in practice despite the high price of Pt. The excellent catalytic activity of Pt/C in an aqueous Na-air battery (NAB) was also reported elsewhere [37]. Unlike Pt/C catalyst, Vulcan showed little difference with no catalyst-HCF in an aqueous NAB. The SEM images in Fig. 39 shows surface morphology of the catalysts-coated and uncoated HCFs. There were a lot of flexible microfibers making up HCF and the randomly stacked carbon fibers gave a porous structure (Fig. 39a). After coating the catalysts mixed with PVDF binder, those particles were uniformly physisorbed on the surface (Fig. 39b, c).

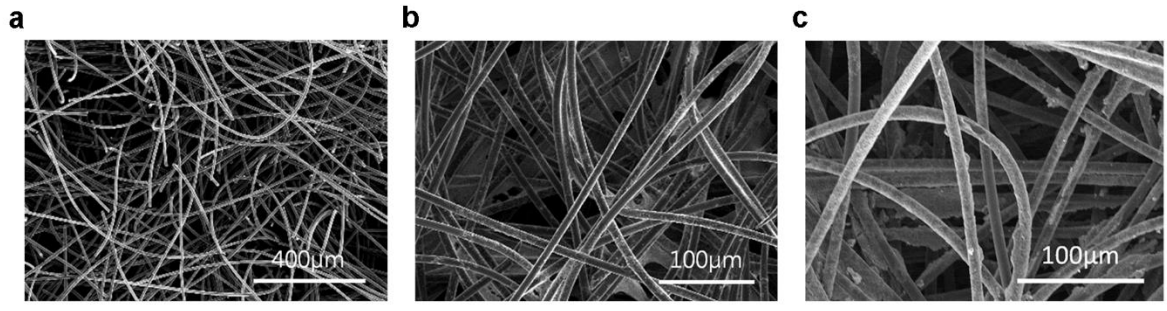

Figure 39. SEM images of carbon felt (a) with and without catalysts such as (b) Pt/C and (c) Vulcan.

Those carbon felt electrodes were employed to a positive electrode with an Na|1M saltwater cell. Fig. 40 exhibits electrochemical performances of the cells, such as voltage efficiency and power density. The galvanostatic charge and discharge were performed at the slower current rate of 0.01 mA/cm^2 than in prior experiments. This was applied to investigate the catalytic effect more precisely (Fig. 40a). As expected, the Pt/C cell showed the smallest overpotential for OER and ORR, exhibiting especially good activity of OER, and markedly superior voltage efficiency of around 0.3 V. The Vulcan cell indicated slightly better voltage efficiency than HCF without catalysts. The similar trend was shown in the result of power density (Fig. 40b). Although an excellent activity of Pt/C catalysts was demonstrated, Pt/C catalysts have a few drawbacks in terms of high price and a degraded catalyst layer due to agglomeration, Pt dissolution and carbon corrosion [108,109]. Therefore, using Pt/C catalysts in the saltwater battery is undesirable and other non-precious catalysts with highly bi-functional activity (for OER and ORR) and good stability are required to improve the cell performances.

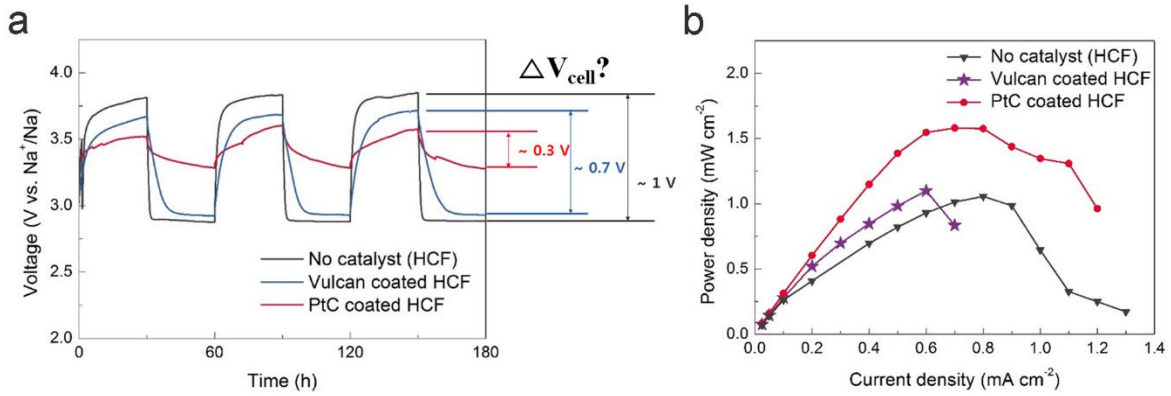

Figure 40. Electrochemical test to investigating influences of catalysts on electrochemical performances of saltwater battery. (a) Galvanostatic charge and discharge voltage curve at 0.01 mA/cm^2 for 180 hours (3 cycles) with half-cells of Na|1M saltwater. (b) Power density at different current density from 0.01 to 0.75 mA/cm^2.

3.4. Cost analysis.

The saltwater batteries are remarkably low-cost in terms of both energy and power production. Fig. 41 illustrates the energy cost versus power cost of various types of batteries for ESS (Table 3). Na-sulphur batteries (NaS) and vanadium redox flow batteries (VRB) have been considered as promising candidates for ESS in addition to LIBs. NaS has an energy cost of 438–477 $/kWh and the energy cost of VRB is higher. However, those cost are still too high to market penetration and it have to be reduced below around 200 $/kWh [110]. The energy cost of the saltwater battery with 5 M NaCl is estimated to be only 189 $/kWh; while Zn-air batteries, the next cheapest candidate, is priced at 310 $/kWh. In addition, the working potential and energy density (up to 423 Wh/kg with 6 M saltwater) of the saltwater battery can be tuned by the salt concentration for different applications. As a conceptually simple energy storage device, this battery using the eco-friendly, low-cost saltwater as the active material will be an optimal building block for large-scale stationary ESS applications.

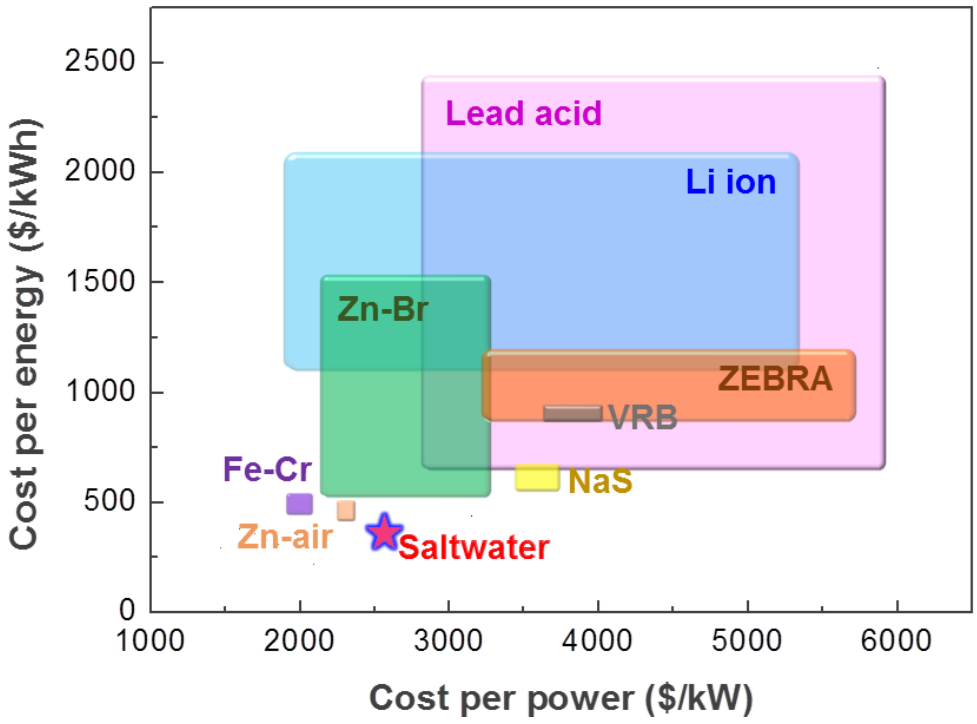

Figure 41. Comparison of cost for various battery systems. Energy cost ($/kWh) versus power cost ($/kW) using data from the DOE/EPRI 2013 Electricity Storage Handbook[3]. The cost of saltwater battery (red star) was evaluated using 5 M saltwater as the catholyte.

Table 3. Cost of various types of batteries for ESS systems used for utility transmission and distribution grid support. The data are from DOE/EPRI 2013 electricity storage handbook [7], except for rechargeable saltwater batteries.

a

Batteries for ESS	Cost	
	$/kW	$/kWh
NaS	3152~3434	438~477
Na-NiCl	2907~5676	727~1135
Vanadium redox flow(VRB)	3335~3756	751~834
Fe-Cr	1473~1596	295~379
Zn-Br	1699~2957	361~1479
Zn-air	1858	310
Lead-Acid	2477~5876	502~2477
Li- ion(LIB)	1388~5265	996~2126
Saltwater(SWB)	2094	218

b

	Zinc air	Saltwater Battery
ES System		
ES Equipment	1,000,000	704,643
ES Installaion	7,500	5,284.82
Enclosures	24,810	17,482.20
Owner Interconnection		
Equipment	367,000	258,604.07
Installation	92,000	64,827.18
Enclosure		
Utility Interconnection		
Equipment	80,400	56,653.32
Installaion	80,400	56,653.32
Site BOP Installation(Civil Only)	1,267	892.78
Total Cost Equipment	1,472,210	1,037,382.82
Total cost Installation	181,167	127,658.10
General Contractor Facilities at 15% ins tall	27,175	19,148.72
Engineering Fees @ 5% install	9,058	6,382.91
Project Contingency application @ 0-15% install	18,117	12,766.02
Process Contingency application @ 0-15% of battery	150,000	105,696.49
Total Plant Cost(TPC) ($)	1,857,727	1,309,035
$/kW	1,858	2,094.46
$/kWh	310	218.17

Table 3a gives the cost range of existing battery types for large-scale ESS applications, using the maximum and minimum values listed in ref. 7. with the exception of the saltwater battery. Table 3b shows the costs breakdown based on vender quotes, such as OEM suppliers, power conditioning system (PCS) provider and system integrators, and financial assumptions. For example, process contingency assumption was applied with considering technology maturity and the level of development and commercialisation of each battery type. The cost of energy storage (ES) equipment in Table 3b, which indicates the material cost of the batteries and the total material cost composed of modules of 40000 kWh in serial-parallel system, is applied to the value of saltwater battery.

To convert from lab to commercial scale, the ES equipment cost of saltwater batteries was reduced by a factor of ten, which is the typical reduction ratio during commercialization. Values other than ES equipment for rechargeable saltwater batteries are hard to calculate, since the batteries are in the stage of research and development. For this reason, values such as PCS cost for the saltwater battery were those of redox flow battery, which is the most similar system. Other values for the saltwater batteries in Table 3b were obtained by assuming the same cost ratio between the ES equipment and other values as that in redox flow battery, except the process contingency cost, which was estimated based on a zinc-air battery that is still in developmental stage.

4. Conclusions.

Battery energy storage systems (BESS) have received considerable attention as green energy harvesting has become more and more important. However, high costs still prevent from market penetration. In this respect, to save cathode material costs, I proposed using saltwater as cathode to store electrical energy. It was the first time that saltwater was not used as electrolyte but as cathode active material. A new cell is required to store electrical energy with new chemicals and accordingly, a novel cell was designed, which consisted of anode material|organic electrolyte|NASICON|saltwater|positive current collector.

The saltwater battery stored electrical energy via an oxygen evolution reaction (OER). Although the occurrence of chlorine evolution is generally known (resulting from electrolysis of saltwater or seawater) it was expected that the OER generated dominantly by the influence of pH and positive electrodes. An accurate investigation of the charge process is required, by using methods such as differential electrochemical mass spectroscopy (DEMS). During discharge, the saltwater battery provided applications through oxygen reduction reaction (ORR).

Various salt concentrations in aqueous solution are a great advantage of the battery. The cell voltages during charge and discharge were changed owing to concentration polarization, which were decreased according to increasing salt concentration. Also, changing salt levels in water enable energy density to be controlled (the maximum of ~423 Wh/kg at 6 M salt water). It ultimately provides the flexibilities of the saltwater battery for different applications.

The electrochemical performances of the saltwater battery were significantly affected by designing cell components such as such as solid electrolyte, positive current collector, catalysts and anode material. The improvement of cell design, especially in positive electrodes and solid electrolyte, must be performed. For example, highly stable solid electrolyte with good Na^+ conductivity must be developed and positive electrodes with low-cost catalysts are required to compete with commercialized products.

By using saltwater as a cathode, the saltwater battery takes additional advantages as a promising energy storage system. Eco-friendly aqueous solution needed no chemical treatment and special reservoirs. Also, the low cost of the cathode material contributed to a strong price competitiveness compared to other battery based energy storage systems. The saltwater would be easier to scale up since it has not only reliable electrochemical performance but also low cost and a simplicity in its electrochemical reactions. In conclusion, these features, as well as the results of this research, suggest a strong possibility of the rechargeable saltwater battery as a next energy storage system.

5. References.

1. Zhang, T.; Imanishi, N.; Takeda, Y.; Yamamoto, O., Aqueous lithium/air rechargeable batteries. *Chemistry Letters* **2011,** *40* (7), 668-673.
2. Xiong, X.; Luo, W.; Hu, X.; Chen, C.; Qie, L.; Hou, D.; Huang, Y., Flexible Membranes of MoS2/C Nanofibers by Electrospinning as Binder-Free Anodes for High-Performance Sodium-Ion Batteries. *Scientific Reports* **2015,** *5*, 9254.
3. Dincer, I., Renewable energy and sustainable development: a crucial review. *Renewable and Sustainable Energy Reviews* **2000,** *4* (2), 157-175.
4. Jacobson, M. Z., Review of solutions to global warming, air pollution, and energy security. *Energy & Environmental Science* **2009,** *2* (2), 148-173.
5. Yang, Z.; Zhang, J.; Kintner-Meyer, M. C.; Lu, X.; Choi, D.; Lemmon, J. P.; Liu, J., Electrochemical energy storage for green grid. *Chemical reviews* **2011,** *111* (5), 3577-3613.
6. Dunn, B.; Kamath, H.; Tarascon, J.-M., Electrical energy storage for the grid: a battery of choices. *Science* **2011,** *334* (6058), 928-935.
7. Akhil, A. A.; Huff, G.; Currier, A. B.; Kaun, B. C.; Rastler, D. M.; Chen, S. B.; Cotter, A. L.; Bradshaw, D. T.; Gauntlett, W. D., *DOE/EPRI 2013 electricity storage handbook in collaboration with NRECA*. Sandia National Laboratories Albuquerque, NM, USA: 2013.
8. Hall, P. J.; Bain, E. J., Energy-storage technologies and electricity generation. *Energy policy* **2008,** *36* (12), 4352-4355.
9. Ibrahim, H.; Ilinca, A.; Perron, J., Energy storage systems—characteristics and comparisons. *Renewable and sustainable energy reviews* **2008,** *12* (5), 1221-1250.
10. Winter, M.; Brodd, R. J., What are batteries, fuel cells, and supercapacitors? *Chemical reviews* **2004,** *104* (10), 4245-4270.
11. McCloskey, B. D., Expanding the Ragone Plot: Pushing the Limits of Energy Storage. *J. Phys. Chem. Lett* **2015,** *6* (18), 3592-3593.
12. Burgess, J.; Burgess, J., *Metal ions in solution*. Ellis Horwood Chichester: 1978.
13. Pan, H.; Hu, Y.-S.; Chen, L., Room-temperature stationary sodium-ion batteries for large-scale electric energy storage. *Energy & Environmental Science* **2013,** *6* (8), 2338-2360.
14. Oshima, T.; Kajita, M.; Okuno, A., Development of Sodium-Sulfur Batteries. *International Journal of Applied Ceramic Technology* **2004,** *1* (3), 269-276.
15. Ellis, B. L.; Nazar, L. F., Sodium and sodium-ion energy storage batteries. *Current Opinion in Solid State and Materials Science* **2012,** *16* (4), 168-177.
16. Hayashi, A.; Noi, K.; Sakuda, A.; Tatsumisago, M., Superionic glass-ceramic electrolytes for room-temperature rechargeable sodium batteries. *Nature communications* **2012,** *3*, 856.
17. Xin, S.; Yin, Y. X.; Guo, Y. G.; Wan, L. J., A High-Energy Room-Temperature Sodium-Sulfur Battery. *Advanced Materials* **2014,** *26* (8), 1261-1265.
18. Jeong, G.; Kim, H.; Lee, H. S.; Han, Y.-K.; Park, J. H.; Jeon, J. H.; Song, J.; Lee, K.; Yim, T.; Kim, K. J., A room-temperature sodium rechargeable battery using an SO2-based nonflammable inorganic liquid catholyte.

Scientific reports **2015,** *5*.

19. Palomares, V.; Casas-Cabanas, M.; Castillo-Martínez, E.; Han, M. H.; Rojo, T., Update on Na-based battery materials. A growing research path. *Energy & Environmental Science* **2013,** *6* (8), 2312-2337.
20. De Leon, C. P.; Frías-Ferrer, A.; González-García, J.; Szánto, D.; Walsh, F. C., Redox flow cells for energy conversion. *Journal of Power Sources* **2006,** *160* (1), 716-732.
21. Weber, A. Z.; Mench, M. M.; Meyers, J. P.; Ross, P. N.; Gostick, J. T.; Liu, Q., Redox flow batteries: a review. *Journal of Applied Electrochemistry* **2011,** *41* (10), 1137-1164.
22. Skyllas-Kazacos, M.; Chakrabarti, M.; Hajimolana, S.; Mjalli, F.; Saleem, M., Progress in flow battery research and development. *Journal of the Electrochemical Society* **2011,** *158* (8), R55-R79.
23. Christensen, J.; Albertus, P.; Sanchez-Carrera, R. S.; Lohmann, T.; Kozinsky, B.; Liedtke, R.; Ahmed, J.; Kojic, A., A critical review of Li/air batteries. *Journal of the Electrochemical Society* **2011,** *159* (2), R1-R30.
24. Lu, J.; Li, L.; Park, J.-B.; Sun, Y.-K.; Wu, F.; Amine, K., Aprotic and aqueous Li–O2 batteries. *Chemical reviews* **2014,** *114* (11), 5611-5640.
25. Bruce, P. G.; Freunberger, S. A.; Hardwick, L. J.; Tarascon, J.-M., Li-O2 and Li-S batteries with high energy storage. *Nature materials* **2012,** *11* (1), 19-29.
26. Abraham, K.; Jiang, Z., A polymer electrolyte-based rechargeable lithium/oxygen battery. *Journal of The Electrochemical Society* **1996,** *143* (1), 1-5.
27. Girishkumar, G.; McCloskey, B.; Luntz, A.; Swanson, S.; Wilcke, W., Lithium− air battery: promise and challenges. *The Journal of Physical Chemistry Letters* **2010,** *1* (14), 2193-2203.
28. Kraytsberg, A.; Ein-Eli, Y., Review on Li–air batteries—Opportunities, limitations and perspective. *Journal of Power Sources* **2011,** *196* (3), 886-893.
29. Wang, Q.; Ping, P.; Zhao, X.; Chu, G.; Sun, J.; Chen, C., Thermal runaway caused fire and explosion of lithium ion battery. *Journal of power sources* **2012,** *208*, 210-224.
30. Manthiram, A.; Li, L., Hybrid and Aqueous Lithium-Air Batteries. *Advanced Energy Materials* **2015,** *5* (4).
31. He, H.; Niu, W.; Asl, N. M.; Salim, J.; Chen, R.; Kim, Y., Effects of aqueous electrolytes on the voltage behaviors of rechargeable Li-air batteries. *Electrochimica Acta* **2012,** *67*, 87-94.
32. Zhou, H.; Wang, Y.; Li, H.; He, P., The development of a new type of rechargeable batteries based on hybrid electrolytes. *ChemSusChem* **2010,** *3* (9), 1009-1019.
33. Ha, S.; Kim, J. K.; Choi, A.; Kim, Y.; Lee, K. T., Sodium–Metal Halide and Sodium–Air Batteries. *ChemPhysChem* **2014,** *15* (10), 1971-1982.
34. Hayashi, K.; Shima, K.; Sugiyama, F., A Mixed Aqueous/Aprotic Sodium/Air Cell Using a NASICON Ceramic Separator. *Journal of The Electrochemical Society* **2013,** *160* (9), A1467-A1472.
35. Liang, F.; Hayashi, K., A High-Energy-Density Mixed-Aprotic-Aqueous Sodium-Air Cell with a Ceramic Separator and a Porous Carbon Electrode. *Journal of The Electrochemical Society* **2015,** *162* (7), A1215-A1219.
36. Hashimoto, T.; Hayashi, K., Aqueous and Nonaqueous Sodium-Air Cells with Nanoporous Gold Cathode. *Electrochimica Acta* **2015,** *182*, 809-814.
37. Sahgong, S. H.; Senthilkumar, S.; Kim, K.; Hwang, S. M.; Kim, Y., Rechargeable aqueous Na–air batteries: Highly improved voltage efficiency by use of catalysts. *Electrochemistry Communications* **2015,** *61*, 53-56.

38. Hartmann, P.; Bender, C. L.; Vračar, M.; Dürr, A. K.; Garsuch, A.; Janek, J.; Adelhelm, P., A rechargeable room-temperature sodium superoxide (NaO2) battery. *Nature materials* **2013,** *12* (3), 228-232.
39. Slater, M. D.; Kim, D.; Lee, E.; Johnson, C. S., Sodium-Ion Batteries. *Advanced Functional Materials* **2013,** *23* (8), 947-958.
40. Chevrier, V.; Ceder, G., Challenges for Na-ion negative electrodes. *Journal of The Electrochemical Society* **2011,** *158* (9), A1011-A1014.
41. Bi, X.; Ren, X.; Huang, Z.; Yu, M.; Kreidler, E.; Wu, Y., Investigating dendrites and side reactions in sodium–oxygen batteries for improved cycle lives. *Chemical Communications* **2015,** *51* (36), 7665-7668.
42. Kim, J. K.; Lee, E.; Kim, H.; Johnson, C.; Cho, J.; Kim, Y., Rechargeable Seawater Battery and Its Electrochemical Mechanism. *ChemElectroChem* **2015,** *2* (3), 328-332.
43. Kim, H.; Park, J.-S.; Sahgong, S. H.; Park, S.; Kim, J.-K.; Kim, Y., Metal-free hybrid seawater fuel cell with an ether-based electrolyte. *Journal of Materials Chemistry A* **2014,** *2* (46), 19584-19588.
44. Kim, J.-K.; Mueller, F.; Kim, H.; Bresser, D.; Park, J.-S.; Lim, D.-H.; Kim, G.-T.; Passerini, S.; Kim, Y., Rechargeable-hybrid-seawater fuel cell. *NPG Asia Materials* **2014,** *6* (11), e144.
45. Abdel-Aal, H.; Sultan, S.; Hussein, I., Parametric study for saline water electrolysis: Part II—Chlorine evolution, selectivity and determination. *International journal of hydrogen energy* **1993,** *18* (7), 545-551.
46. Abdel-Aal, H.; Zohdy, K.; Kareem, M. A., Hydrogen Production Using Sea Water Electrolysis. *The Open Fuel Cells Journal* **2010,** *3*, 1-7.
47. Stevens, D.; Dahn, J., High Capacity Anode Materials for Rechargeable Sodium-Ion Batteries. *Journal of the Electrochemical Society* **2000,** *147* (4), 1271-1273.
48. Li, Y.; Xu, S.; Wu, X.; Yu, J.; Wang, Y.; Hu, Y.-S.; Li, H.; Chen, L.; Huang, X., Amorphous monodispersed hard carbon micro-spherules derived from biomass as a high performance negative electrode material for sodium-ion batteries. *Journal of Materials Chemistry A* **2015,** *3* (1), 71-77.
49. Xu, Y.; Zhu, Y.; Liu, Y.; Wang, C., Electrochemical Performance of Porous Carbon/Tin Composite Anodes for Sodium-Ion and Lithium-Ion Batteries. *Advanced Energy Materials* **2013,** *3* (1), 128-133.
50. Zhu, H.; Jia, Z.; Chen, Y.; Weadock, N.; Wan, J.; Vaaland, O.; Han, X.; Li, T.; Hu, L., Tin anode for sodium-ion batteries using natural wood fiber as a mechanical buffer and electrolyte reservoir. *Nano letters* **2013,** *13* (7), 3093-3100.
51. Brown, E.; Colling, A.; Park, D.; Phillips, J.; Rothery, D.; Wright, J., *Seawater: its composition, properties and behaviour*. Butterworth-Heinemann: 1995.
52. Robinson, R. A.; Stokes, R. H., *Electrolyte solutions*. Courier Corporation: 2002.
53. Nestoridi, M.; Pletcher, D.; Wood, R. J.; Wang, S.; Jones, R. L.; Stokes, K. R.; Wilcock, I., The study of aluminium anodes for high power density Al/air batteries with brine electrolytes. *Journal of Power Sources* **2008,** *178* (1), 445-455.
54. Jeong, Y.; Manthiram, A., Nanocrystalline manganese oxides for electrochemical capacitors with neutral electrolytes. *Journal of the Electrochemical Society* **2002,** *149* (11), A1419-A1422.
55. 김윤호 *Study on Ionic Conduction and Degradation Mechanisms on Super-ionic Conductor*; Korea Institute Of Science and Technology 1991-08, 1991.

56. Hummers Jr, W. S.; Offeman, R. E., Preparation of graphitic oxide. *Journal of the American Chemical Society* **1958,** *80* (6), 1339-1339.
57. Peng, Z.; Freunberger, S. A.; Hardwick, L. J.; Chen, Y.; Giordani, V.; Bardé, F.; Novák, P.; Graham, D.; Tarascon, J. M.; Bruce, P. G., Oxygen Reactions in a Non-Aqueous Li+ Electrolyte. *Angewandte Chemie* **2011,** *123* (28), 6475-6479.
58. Xu, W.; Xiao, J.; Zhang, J.; Wang, D.; Zhang, J.-G., Optimization of nonaqueous electrolytes for primary lithium/air batteries operated in ambient environment. *Journal of the Electrochemical Society* **2009,** *156* (10), A773-A779.
59. Cho, M.; Trottier, J.; Gagnon, C.; Hovington, P.; Clément, D.; Vijh, A.; Kim, C.-S.; Guerfi, A.; Black, R.; Nazar, L., The effects of moisture contamination in the Li-O 2 battery. *Journal of Power Sources* **2014,** *268*, 565-574.
60. Zhang, T.; Zhou, H., A reversible long-life lithium–air battery in ambient air. *Nature communications* **2013,** *4*, 1817.
61. Manthiram, A.; Li, L.; Zhao, X. In *A Dual-Electrolyte Rechargeable Li-Air Battery with Phosphate Buffer Catholyte*, Meeting Abstracts, The Electrochemical Society: 2012; pp 479-479.
62. Fergus, J. W., Ion transport in sodium ion conducting solid electrolytes. *Solid State Ionics* **2012,** *227*, 102-112.
63. Anantharamulu, N.; Rao, K. K.; Rambabu, G.; Kumar, B. V.; Radha, V.; Vithal, M., A wide-ranging review on Nasicon type materials. *Journal of materials science* **2011,** *46* (9), 2821-2837.
64. Lee, S.-M.; Lee, S.-T.; Lee, D.-H.; Lee, S.-H.; Han, S.-S.; Lim, S.-K., Effect of particle size on the density and ionic conductivity of Na3Zr2Si2PO12 NASICON. *Journal of Ceramic Processing Research* **2015,** *16* (1), 49-53.
65. Bohnke, O.; Ronchetti, S.; Mazza, D., Conductivity measurements on nasicon and nasicon-modified materials. *Solid State Ionics* **1999,** *122* (1), 127-136.
66. Will, F., Effect of water on beta alumina conductivity. *Journal of The Electrochemical Society* **1976,** *123* (6), 834-836.
67. Liu, M.; De Jonghe, L. C., Chemical Stability of Sodium Beta ″-Alumina Electrolyte in Sulfur/Sodium Polysulfide Melts. *Journal of The Electrochemical Society* **1988,** *135* (3), 741-749.
68. Fuentes, R.; Figueiredo, F.; Marques, F.; Franco, J., Reaction of NASICON with water. *Solid State Ionics* **2001,** *139* (3), 309-314.
69. Goodenough, J.; Hong, H.-P.; Kafalas, J., Fast Na+-ion transport in skeleton structures. *Materials Research Bulletin* **1976,** *11* (2), 203-220.
70. Boilot, J.; Collin, G.; Colomban, P., Crystal structure of the true nasicon: Na 3 Zr 2 Si 2 PO 12. *Materials research bulletin* **1987,** *22* (5), 669-676.
71. Von Alpen, U.; Bell, M.; Höfer, H., Compositional dependence of the electrochemical and structural parameters in the Nasicon system (Na 1+ x Si x Zr 2 P 3− x O 12). *Solid State Ionics* **1981,** *3*, 215-218.
72. Ahmad, A.; Wheat, T.; Kuriakose, A.; Canaday, J.; McDonald, A., Dependence of the properties of Nasicons on their composition and processing. *Solid State Ionics* **1987,** *24* (1), 89-97.
73. Mauvy, F.; Siebert, E.; Fabry, P., Reactivity of NASICON with water and interpretation of the detection limit of a NASICON based Na+ ion selective electrode. *Talanta* **1999,** *48* (2), 293-303.

74. Bunker, B., Molecular mechanisms for corrosion of silica and silicate glasses. *Journal of Non-Crystalline Solids* **1994,** *179*, 300-308.
75. Ignaszak, A.; Pasierb, P.; Komornicki, S., The effect of humidity on the electrical properties of Nasicon-type materials. *MATERIALS SCIENCE-WROCLAW-* **2006,** *24* (1), 95.
76. Kang, H.-B.; Cho, N.-H., Phase formation, sintering behavior, and electrical characteristics of NASICON compounds. *Journal of materials science* **1999,** *34* (20), 5005-5013.
77. Kuriakose, A.; Wheat, T.; Ahmad, A.; Dirocco, J., Synthesis, sintering, and microstructure of NASICONS. *Journal of the American Ceramic Society* **1984,** *67* (3), 179-183.
78. Komorowski, P.; Argyropoulos, S.; Hancock, R.; Gulens, J.; Taylor, P.; Canaday, J.; Kuriakose, A.; Wheat, T.; Ahmad, A., Characterization of protonically exchanged NASICON. *Solid State Ionics* **1991,** *48* (3), 295-301.
79. Franco, A. A.; Xue, K.-H., Carbon-based electrodes for lithium air batteries: scientific and technological challenges from a modeling perspective. *ECS Journal of Solid State Science and Technology* **2013,** *2* (10), M3084-M3100.
80. Chakrabarti, M.; Brandon, N.; Hajimolana, S.; Tariq, F.; Yufit, V.; Hashim, M.; Hussain, M.; Low, C.; Aravind, P., Application of carbon materials in redox flow batteries. *Journal of Power Sources* **2014,** *253*, 150-166.
81. Kim, K. J.; Park, M.-S.; Kim, Y.-J.; Kim, J. H.; Dou, S. X.; Skyllas-Kazacos, M., A technology review of electrodes and reaction mechanisms in vanadium redox flow batteries. *Journal of Materials Chemistry A* **2015,** *3* (33), 16913-16933.
82. Litster, S.; McLean, G., PEM fuel cell electrodes. *Journal of Power Sources* **2004,** *130* (1), 61-76.
83. Bourke, A.; Miller, M.; Lynch, R.; Gao, X.; Landon, J.; Wainright, J.; Savinell, R.; Buckley, D., Electrode Kinetics of Vanadium Flow Batteries: Contrasting Responses of VII-VIII and VIV-VV to Electrochemical Pretreatment of Carbon. *Journal of The Electrochemical Society* **2016,** *163* (1), A5097-A5105.
84. Noack, J.; Tübke, J., A comparison of materials and treatment of materials for vanadium redox flow battery. *ECS Transactions* **2010,** *25* (35), 235-245.
85. Dreyer, D. R.; Park, S.; Bielawski, C. W.; Ruoff, R. S., The chemistry of graphene oxide. *Chemical Society Reviews* **2010,** *39* (1), 228-240.
86. Li, W.; Liu, J.; Yan, C., Reduced graphene oxide with tunable C/O ratio and its activity towards vanadium redox pairs for an all vanadium redox flow battery. *Carbon* **2013,** *55*, 313-320.
87. Han, P.; Wang, H.; Liu, Z.; Chen, X.; Ma, W.; Yao, J.; Zhu, Y.; Cui, G., Graphene oxide nanoplatelets as excellent electrochemical active materials for VO 2+/and V 2+/V 3+ redox couples for a vanadium redox flow battery. *Carbon* **2011,** *49* (2), 693-700.
88. Seredych, M.; Tamashausky, A. V.; Bandosz, T. J., Graphite oxides obtained from porous graphite: the role of surface chemistry and texture in ammonia retention at ambient conditions. *Advanced Functional Materials* **2010,** *20* (10), 1670-1679.
89. Wei, D.; Liu, Y.; Wang, Y.; Zhang, H.; Huang, L.; Yu, G., Synthesis of N-doped graphene by chemical vapor deposition and its electrical properties. *Nano letters* **2009,** *9* (5), 1752-1758.
90. Shao, Y.; Zhang, S.; Engelhard, M. H.; Li, G.; Shao, G.; Wang, Y.; Liu, J.; Aksay, I. A.; Lin, Y., Nitrogen-doped graphene and its electrochemical applications. *Journal of Materials Chemistry* **2010,** *20* (35), 7491-7496.

91. Kim, K. J.; Lee, S.-W.; Yim, T.; Kim, J.-G.; Choi, J. W.; Kim, J. H.; Park, M.-S.; Kim, Y.-J., A new strategy for integrating abundant oxygen functional groups into carbon felt electrode for vanadium redox flow batteries. *Scientific reports* **2014,** *4*.

92. Sun, B.; Skyllas-Kazacos, M., Modification of graphite electrode materials for vanadium redox flow battery application—I. Thermal treatment. *Electrochimica Acta* **1992,** *37* (7), 1253-1260.

93. Pezeshki, A. M.; Clement, J. T.; Veith, G. M.; Zawodzinski, T. A.; Mench, M. M., High performance electrodes in vanadium redox flow batteries through oxygen-enriched thermal activation. *Journal of Power Sources* **2015,** *294*, 333-338.

94. Ohkuma, H.; Uechi, I.; Matsui, M.; Takeda, Y.; Yamamoto, O.; Imanishi, N., Stability of carbon electrodes for aqueous lithium-air secondary batteries. *Journal of Power Sources* **2014,** *245*, 947-952.

95. Brett, C. M.; Brett, A. M. O., *Electrochemistry: principles, methods, and applications*. Oxford university press Oxford: 1993; Vol. 4.

96. *전기화학(2판)*. 자유아카데미: 2014.

97. Pourbaix, M., Atlas of electrochemical equilibria in aqueous solutions. **1974**.

98. Chen, S.; Zheng, Y.; Wang, S.; Chen, X., Ti/RuO 2–Sb 2 O 5–SnO 2 electrodes for chlorine evolution from seawater. *Chemical Engineering Journal* **2011,** *172* (1), 47-51.

99. Zeradjanin, A. R.; Menzel, N.; Schuhmann, W.; Strasser, P., On the faradaic selectivity and the role of surface inhomogeneity during the chlorine evolution reaction on ternary Ti–Ru–Ir mixed metal oxide electrocatalysts. *Physical Chemistry Chemical Physics* **2014,** *16* (27), 13741-13747.

100. Makarova, M. V.; Jirkovský, J.; Klementová, M.; Jirka, I.; Macounová, K.; Krtil, P., The electrocatalytic behavior of Ru 0.8 Co 0.2 O 2− x—the effect of particle shape and surface composition. *Electrochimica Acta* **2008,** *53* (5), 2656-2664.

101. Wong, R. W. M. a. C. S. *The interaction of chlorine and seawater*; Institute of Ocean Sciences. Patrica Bay Victoric, B.C.: 02,1977, pp 6-7.

102. Siebert, E.; Caneiro, A.; Fabry, P.; Levy, M., Na+ exchange at the NASICON/water interface. *Journal of Electroanalytical Chemistry and Interfacial Electrochemistry* **1990,** *286* (1), 245-251.

103. Water Density Calculator. http://www.csgnetwork.com/h2odenscalc.html.

104. Cramer, S. D., The solubility of oxygen in brines from 0 to 300 C. *Industrial & Engineering Chemistry Process Design and Development* **1980,** *19* (2), 300-305.

105. Stevens, D.; Dahn, J., The mechanisms of lithium and sodium insertion in carbon materials. *Journal of The Electrochemical Society* **2001,** *148* (8), A803-A811.

106. Irisarri, E.; Ponrouch, A.; Palacin, M., Review—Hard Carbon Negative Electrode Materials for Sodium-Ion Batteries. *Journal of The Electrochemical Society* **2015,** *162* (14), A2476-A2482.

107. Cao, R.; Lee, J. S.; Liu, M.; Cho, J., Recent Progress in Non-Precious Catalysts for Metal-Air Batteries. *Advanced Energy Materials* **2012,** *2* (7), 816-829.

108. Zhang, J., *PEM fuel cell electrocatalysts and catalyst layers: fundamentals and applications*. Springer Science & Business Media: 2008.

109. Roen, L.; Paik, C.; Jarvi, T., Electrocatalytic corrosion of carbon support in PEMFC cathodes.

Electrochemical and Solid-State Letters **2004,** *7* (1), A19-A22.

110. Kim, H.; Boysen, D. A.; Newhouse, J. M.; Spatocco, B. L.; Chung, B.; Burke, P. J.; Bradwell, D. J.; Jiang, K.; Tomaszowska, A. A.; Wang, K., Liquid metal batteries: Past, present, and future. *Chemical reviews* **2012,** *113* (3), 2075-2099.

6. Acknowledgements.

먼저 대학원 2년 동안 믿고 지원해주신 부모님께 감사 드립니다. "사랑합니다. 아빠! 엄마!" 목표하는 곳에 취업하여 꼭 효도하겠습니다. 사랑하는 동생 상은이, 논문 그림 준비할 때 도움을 받았는데 너무 고맙고 자랑스럽다. 학업과 연구에 집중할 수 있도록 걱정 안 시킨 상중이도 고마워.

랩의 초창기 멤버로서 김영식 교수님의 지도 하에, 스스로 연구를 수행하며 2년 전보다 일적으로나 개인적으로나 많이 성장했습니다. 특히나, 교수님께서 창의적으로 생각하시는 모습과 일에 대한 추진력과 통찰력을 보며 삶의 자세에 대해 많은 것들은 배울 수 있었습니다. "교수님, 그 동안 잘 지도해주셔서 감사합니다. 존경합니다!" 바쁘신 와중에도 학위 논문 심사에 참여해주시고 좋은 말씀 해주신 최남순 교수님, 강석주 교수님께도 감사 드립니다.

유니스트 입학으로, 처음으로 집을 떠나 타지에 머물며 입학 초반에는 정말 힘들었습니다. 이 때, 함께 고생하고 도와준 내동생 정선이, 걸그룹 효진오빠, 터프한 선혜 그리고 수빈이, 자영언니, 병환오빠, 예원이, 왕근&태승오빠 너무 고마워요. 저희 랩은 프로젝트를 개별적으로 수행하므로 연구에 막힐 때마다 김경호 박사님, 황수민 박사님께서 도움이 되는 조언들을 해주셨습니다. 박사님들 감사 드립니다. 김경호 박사님께서는 저 뿐만 아니라 랩 학생들에게 살아가는데 도움이 되는 말씀 그리고 힘이 되는 말씀을 항상 해주셔서 힘들 때 많이 용기를 얻었습니다. 그리고 황수민 박사님께서는 실험 방법부터 시작해서 논문 작성까지 주옥 같은 조언들을 많이 해주셨습니다.

가족 같은 분위기의 우리 YK Group 랩원들, 소녀감성 대겸오빠, 등대 같은 용일오빠, 항상 밝은 진협오빠, 천사 현지언니, 팔방미남 현우오빠, 에이스 영준이, 솔선수범 준수, 매력터지는 성우, 멘탈갑 현태, 신입 우석이 너무 고맙습니다. 다들 열심히 하니까 곧 좋은 결실 맺을 거라고 믿습니다. 최근 모두 함께 해수전지 모듈을 만들면서, 고생은 많이 했지만, 랩원들이 단합하여 성과를 냈던 하나의 추억이 생겨 개인적으로 기쁩니다. 논문 준비와 진로 걱정 그리고 졸업 준비를 하면서 스트레스로 힘겨워할 때나 힘겨워 포기하고 싶을 때, 지영오빠가 이야기를 들어주고 응원해주었기에 무엇이든 포기하지 않고 잘 마무리할 수 있었습니다. "고마워 오빠!" 마지막으로 최고의 룸메이트, 언영이, 비록 룸메이트가 된지는 오래지 않았지만 동생임에도 불구하고 배울 점이 참 많고 가끔 이야기도 들어주고 항상 챙겨주어 고마워요!.

학위와 성과뿐만 아니라, 좋은 사람들을 만나 보고 느끼며 제가 2 년 전에 비해 너무나 성장할 수 있었습니다. 여러분들 덕분에 제가 석사 학위를 받을 수 있었다고 생각하며, 추후에 석사 기간을 떠올리더라도 웃음지을 수 있을 것 같습니다. 다시 한번 감사 드립니다. 다들 원하시는 목표를 달성하시고 무엇보다 건강하고 행복하시길 바랍니다.